CHALMERS
UNIVERSITY OF TECHNOLOGY

# Rejecting P and CP-invariance in scalar dark matter-nucleus interactions

Master's thesis in physics

JOAKIM HAGEL

Department of Physics
CHALMERS UNIVERSITY OF TECHNOLOGY
Gothenburg, Sweden 2020

MASTER'S THESIS 2020

# Rejecting P and CP-invariance in scalar dark matter-nucleus interactions

JOAKIM HAGEL

CHALMERS
UNIVERSITY OF TECHNOLOGY

Department of Physics
*Division of Subatomic, High Energy and Plasma Physics*
Theoretical Astroparticle Physics
CHALMERS UNIVERSITY OF TECHNOLOGY
Gothenburg, Sweden 2020

Rejecting P and CP-invariance in scalar dark matter-nucleus interactions
JOAKIM HAGEL



Supervisor: Ricardo Catena, Department of Pysics
Examiner: Gabriel Ferretti, Department of Physics

Master's Thesis 2020
Department of Physics
Division of Subatomic, High Energy and Plasma Physics
Theoretical Astroparticle Physics
Chalmers University of Technology
SE-412 96 Gothenburg
+46702062907

Typeset in LaTeX
Printed by Chalmers Reproservice
Gothenburg, Sweden 2020

Rejecting P and CP-invariance in scalar dark matter-nucleus ineractions
JOAKIM HAGEL
Department of Physics
Chalmers University of Technology

# Abstract

There is convincing evidence that a significant fraction of the mass in our Universe consists of non-baryonic and non-luminous dark matter. The particles forming this cosmological component have so far escaped detection, but are currently searched for at direct detection experiments. These search for non-relativistic dark matter-nucleus scattering events in low-background, deep underground detectors. In this thesis, the properties of spin-0 dark matter-nucleus interactions under P and CP-transformations are investigated, assuming that a dark matter signal has been observed at direct detection experiments. Using an effective theory to describe these interactions, the scattering events can be restricted to three cases: Conserving CP and P; Conserving CP, but violating P; and violating both CP and P. By performing a likelihood ratio test with simulated data, this thesis aims to determine how many observed scattering events are required in order to discriminate one case from the other in the next generation of direct detection experiments.

Keywords: High Energy Physics, Dark Matter, Effective Theory, Direct Detection, P and CP-transformations

# Acknowledgements

First and foremost, I would like to thank my supervisor Riccardo Catena for his constant support during this master thesis project. I am both grateful for the valuable feedback and advice I have received during this thesis, and the help I got on the administrative side as well. Without that help, this thesis project would not have been possible.

I would also like to extend my thanks to the rest of the group, with a special thank you to Timon Emken. Your constant willingness to engage in conversation and lend useful advice has helped this project greatly.

Last, but not least I would like to thank my family. Without their help moving across the entire country, this thesis project would not have happened.

Joakim Hagel, Gothenburg, 2020

# Contents

# List of Figures

# List of Tables

# 1

# Introduction

There is convincing evidence that the majority of the mass fraction in the universe consists of non-baryonic dark matter. One promising candidate is the weakly interacting massive particle (WIMP). If such a particle exists it has yet to be discovered. However, a large portion of the parameter space for WIMPs remains unexplored and upcoming experiments will greatly increase the parts of this space that can be searched. One example of such an experiment is the LUX-ZEPLIN experiment, which will start collecting data in 2020 [14].

If searches for signals of dark matter-nucleus scattering events in a deep underground detector were to discover dark matter. That is a discovery of dark matter with direct detection experiments, such as the LUX-ZEPLIN and XENONnT, it is of interest to ask the question what more we can learn from such a discovery about the nature of dark matter [14, 16]. In this thesis, we calculate how many observed events are required in order to discriminate between parity (P) and charge conjugation-parity (CP) transformation properties.

The dark matter-nucleus scatterings that would occur in such an experiment can be modelled using an effective field theory. If we impose the constraint of only considering scalar dark matter on this effective theory, it is possible to reduce the interactions into four different effective operators corresponding to three distinct cases of behaviour under $P$ and $CP$. This in turn allows us to formulate a hypothesis test based on these properties. If the null hypothesis corresponds to even under both $P$ and $CP$, and if the two alternatives corresponds to odd under $P$ and even under $CP$, or odd under $P$ and odd under $CP$, a distribution for a test statistic $q$ can be generated via Monte Carlo simulations. This distribution of the test statistic $q$, which is based on likelihood ratio tests, can then be integrated in order to yield a $P$-value, which in turn gives the significance, with which the null hypothesis can be rejected.

Iterating this statistical test, it is then possible to determined how many scattering events are required in order to reject the hypothesis that scalar dark matter-nucleus interactions are invariant under $P$ and $CP$ in favour for one of the alternatives.

# 2

# Background

In this section, the subject of dark matter is introduced. This includes a brief review of the history and the main evidence for dark matter. In addition, different dark matter candidates and models are listed as well as various different experimental techniques for detecting it.

## 2.1 History and evidence of dark matter

There is a longstanding tradition amongst physicists to understand the dynamics of astronomical objects. This is illustrated by the fact that many refer to Galileo and his observations as the birth of modern observational science. One of the things he discovered was that the faint glow in the night sky from the milky way actually was composed of a great number of stars. Another discovery he made was the previously unseen satellites around the orbit of Jupiter. These discoveries carried with them two important lessons that relates to the modern dark matter problem. The galaxy may contain matter which under normal circumstances would be invisible to us and with new technology it may be possible to observe this matter [8].

### 2.1.1 Galaxy clusters

In 1933, the Swiss-American astronomer Fritz Zwicky studied the redshifts of different galaxy clusters. Within the Coma Cluster, he noticed a large discrepancy concerning the velocity dispersion of galaxies. By applying the virial theorem he could estimate the total mass of the cluster. He then found that 800 galaxies of approximate $10^9$ solar masses in a sphere with $10^6$ light years in radius should have a velocity dispersion of 80 km/s. Instead the observed average velocity dispersion in the line of sight was approximately 1000 km/s. He then concluded that if this discrepancy could be confirmed, the majority of matter in the galaxies would in fact not be luminous, but would be dark matter instead [8].

He then later returned to the virial theorem and tried to estimate the mass of galaxies instead. This time assuming that the Coma cluster had approximately 1000 galaxies within a $2 \cdot 10^6$ light-year radius. With a observed velocity dispersion of 700 km/s, he then solved for the average galaxy mass. Finding a lower limit for the mass of the Coma cluster at $4.5 \cdot 10^{13}$ $M_\odot$, where $M_\odot$ is the symbol for solar mass, he then found that the average galaxy mass was about $4.5 \cdot 10^{10}$ $M_\odot$. Assuming an average luminosity for the galaxy at $8.5 \cdot 10^7$ times that of the sun then yielded a mass-to-light ratio of approximately 500. Since this work was dependent on the work of Hubble, Fritz Zwicky used the value of Hubble constant available at the time and thus overestimated this value by a factor of 8.3. Even with this correction, the mass-to-light ratio indicates that the majority of matter in the galaxy clusters are in fact dark [8].

### 2.1.2 Rotation curves

In 1970, Kent Ford and Vera Rubin published observations made of the rotation curve for the M31 (Andromeda) galaxy. These observations were an improvement in terms of quality when observing rotation curves for spiral galaxies. The same year the astronomer Ken Freeman compared the theoretical prediction of rotation curves for the M33 galaxy to the observed rotational velocity (see figure 2.1). Assuming an exponential disk with a fitted length scale for the current observations, he found that the peak of the rotation curve was at a larger radii than predicted. This led to the conclusion that there must be additional matter. This additional matter could then either not be detected optically or at the current measurement scale. He also arrived at the conclusion that the missing mass would need to be at least as large as the the detected mass in the galaxy [8].

Rotation curves for galaxies are most often calculated via Newtionan dynamics as in eq. (2.1) [9].

$$v(r) = \sqrt{\frac{GM(r)}{r}} \tag{2.1}$$

Where $M(r)$ is given by eq. (2.2) [9].

$$M(r) = 4\pi \int \rho(r) r^2 dr \tag{2.2}$$

Here $\rho(r)$ is the mass density profile. Beyond the optical disc the rotational velocity should be proportional to the the root of the inverse radius, i.e $v(r) \propto 1/\sqrt{r}$. Observations however strongly suggests that the velocity profile is approximately constant. This in turn would indicate the presence of an invisible halo with $\rho(r) \propto 1/r^2$, which in turn then strongly suggests the presence of dark matter [9]. An example of this based on observations is given in figure 2.2.

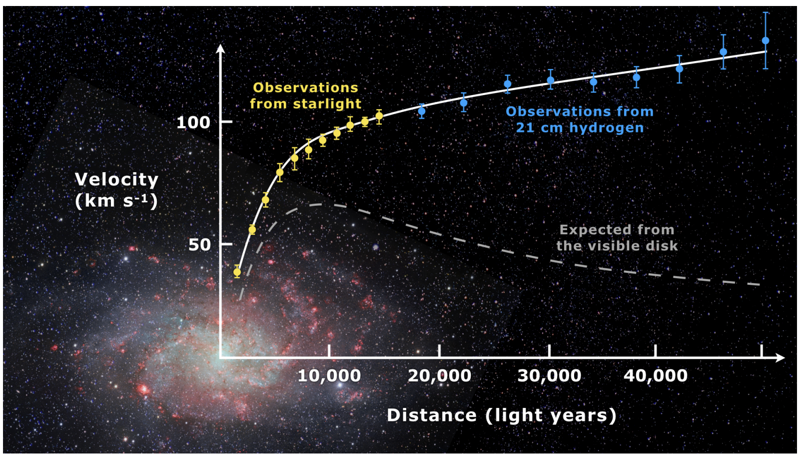


Figure 2.1: Expected rotation curve for the Messier 33 galaxy plotted against the observed rotation curve [1] (public access).

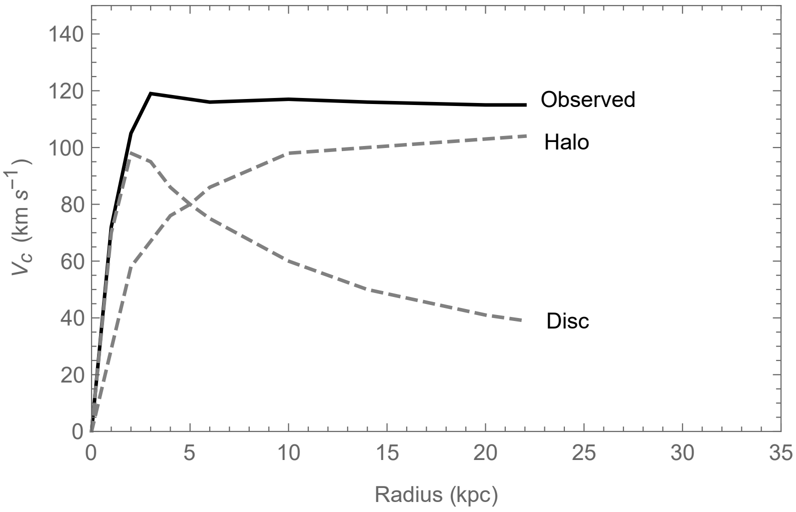


Figure 2.2: Plot over the disc contribution for the observed circular velocity and the dark matter halo contribution needed in order to fit the observed data for the NGC 6503 galaxy. Data from [28].

### 2.1.3 Gravitational lensing and the bullet cluster

One of the strongest pieces of evidence for the existence of dark matter is via gravitational lensing, especially in the case of the observations made by NASA's Chandra X-ray Observatory seen in figure 2.3. By studying the background galaxies via gravitational lensing it is possible to make a map of the gravity and the mass distribution in a galaxy cluster. Furthermore, this observatory took X-ray images of two galaxy clusters colliding, commonly known as the bullet cluster and trough gravitational lensing discovered that the majority of the gravity present did not come from ordinary baryonic matter, but would need to come from matter that does not directly interacts with itself or the hot baryonic gas (at least not strongly). This in turn strongly suggests that some form of dark matter is in fact present in the colliding galaxy clusters [40].

### 2.1.4 Microwave background radiation

Today, one of the leading hypothesis is that the roughly 80% of the total matter in the universe is dark. By the late 1990's, due to advances relating to nucleosynthesis, constraints on the total baryon budget in the universe had been put. These constraints estimated that the total baryon mass fraction could not exceed 20%, thus making the leading hypothesis that dark matter was made of non-baryonic matter [8].

One additional stringent constraint on the baryonic content in the Universe was put by the observation made from the Wilkinson Microwave Anisotropy Probe (WMAP), which measured the background microwave radiation (see figure 2.4). Since the background radiation originated from the decoupling of matter, constraints on the fraction of baryons can be put. This is done by assuming a cosmological model with a fixed number of parameters, then finding the best-fit parameters from looking

Figure 2.3: Composite image of the bullet cluster. The x-ray image (pink areas) show were most of the ordinary baryonic matter is located, which in the collision was slowed down due to interactions. The blue areas show were most of the mass is present via gravitational lensing. The image is superimposed over a background optical image. (Credit goes to: X-ray: NASA/CXC/CfA/M.Markevitch et al.; Optical: NASA/STScI; Magellan/U.Arizona/D.Clowe et al.; Lensing Map: NASA/STScI; ESO WFI; Magellan/U.Arizona/D.Clowe et al.). Image taken from [40].

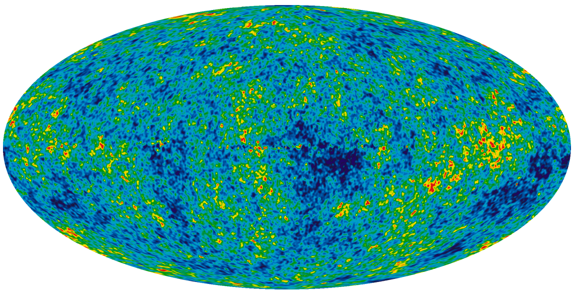

Figure 2.4: Data from WMAP (Credit goes to the WMAP team at NASA) [2].

at the N-dimensional likelihood function. By conducting this analysis of the WMAP data, one found the fraction of baryons should not exceed 20% [9].

$$\Omega_b h^2 = 0.024 \pm 0.001, \quad \Omega_M h^2 = 0.14 \pm 0.02 \tag{2.3}$$

where $\Omega_b h^2$ and $\Omega_M h^2$ are the parameters for baryon density and total mass density [9, 31].

## 2.2 Dark matter candidates

In this section some of the most popular dark matter candidates are briefly reviewed, including some of the potential strengths and weaknesses of the proposed model.

### 2.2.1 Weakly interacting massive particles

One of the leading dark matter candidates is the so called weakly interacting massive particle (WIMP). The WIMP hypothesis grew out of the many proposed dark matter models in the 1980s and 1990s. Many of these models seemed to have similar characteristics. Nearly all being non-baryonic particles heavy enough so they could chemically decouple from the thermal bath in the early stages of the universe. That mass then being heavier than $1 - 100$ keV [8].

If this type of particle was to match the observed cosmological density of dark matter, it would have to self-annihilate with a cross section around $\sigma v$ $10^{-26}$ cm$^3$/s, where $v$ is the dark matter particle relative velocity. This cross section is comparable to that of typical weak scale processes. This, in combination with the theoretical arguments for new physics around the electroweak scale, made this class of particles into the leading hypothesis [8, 45].

Searches for this type of particle has been conducted, both with direct detection methods and collider methods (section 2.3) and no conclusive sign has been seen so far. The DAMA experiment do claim to have measured an annual modulation signal in the rate of nucleus scattering events, as expected from WIMP-nucleus scatterings [7]. Strong tensions have however been found in comparison with other experiments [4, 11].

In 2020 the LUX-ZEPLIN experiment will begin to collect data and thus explore more of the parameter space of possible WIMP particles [14]. Another upcoming experiment is the XENONnT experiment [16].

### 2.2.2 Axions

Axions were first proposed as a solution to the strong $CP$ problem in quantum chromodynamics and have gained traction in later years as a potential dark matter candidate [42]. These particles are expected to have extremely small masses, lower than 0.01 eV and be very weakly interacting. Several axion models exist that satisfy all the current constraints on these particles [9, 42]. This includes constraints put by astrophysics, cosmology and "light shining through a wall" experiments [24].

### 2.2.3 Sterile neutrinos

In 1993, Dodelson and Widrow proposed sterile neutrinos as a potential dark matter candidate [19]. These particles would be similar to ordinary neutrinos in the Standard Model, but not interact via the weak interaction. Today there are strong constraints on these hypothetical dark matter candidates that comes from studies of their cosmological abundance and decay products. Typically, sterile neutrinos are warm dark matter candidates, as most proposed models suggests that they decoupled relativistically from the thermal bath in the early universe. However, sterile neutrinos are also a candidate for cold dark matter, which would mean that they moved non-relativistically in the early epochs of the universe [9, 10, 44].

### 2.2.4 Other proposed models

There is convincing evidence that dark matter is not made of baryonic matter. One proposed alternative to this are primordial black holes, that is black holes that were formed before the nucleosynthesis. These black holes would then have masses below the current microlensing surveys. A lower limit on their mass can be put from constraints provided by the lack of gamma rays from Hawking radiation. One problem with this model is the predicted formation rate for these black holes. In order to get a relevant abundance one has to assume a large degree of non-gaussianity [8].

Another way that has been proposed in order to solve the dark matter problem is trough modified gravity. With this model, no extra mass would be needed at all. This model however fails to provide a satisfactory explanation for the dynamics of galaxy clusters, i.e the bullet cluster [8].

## 2.3 Experimental techniques

This section discusses two major experimental techniques in the search for dark matter, and more specifically in the search for WIMPs. These are the direct detection technique and indirect detection technique.

### 2.3.1 Direct detection

One of the most promising ways of searching for dark matter particles is via the direct detection method, and it is this experimental technique that this thesis is focused on. The principle behind these experiments is simple. If a galactic halo is filled with dark matter particles, some of these particles should pass through earth and it would then be possible to study these particle interactions with matter on earth. By measuring the recoil energy from dark matter-nucleus scatterings it would then be possible to identify these particles [9, 30].

If the direct detection experiment in question covers the parameters space for a real dark matter particle present in the galactic halo, then an annual modulation signal should appear. This signal is due to the earths velocity being parallel and anti-parallel with the sun's motion through the milky way and should thus peak in June and have its minimum in December [27].

The event rate in these experiments is dependent on the density of WIMPs, the velocity distribution of WIMPs and the WIMP-nucleus scattering cross section [9],

$$R \propto N n_\chi < \sigma_\chi > . \tag{2.4}$$

Here $N$ is the detector mass divided by the mass of the target nuclei and $n_\chi$ is the WIMP energy density divided by the WIMP mass.

The local dark matter density is usually estimated to be around 0.3 GeV/cm$^3$ [41] and the velocity distribution is often assumed to be a Maxwell-Boltzmann distribution centered around 270 km/s, this is the same as assuming an isothermal dark matter profile [9].

The cross section in turn is dependent on the particle nature of the WIMP and the scattering kinematics. This has made it convenient to classify different types of scattering processes as elastic or inelastic, and spin-dependent or spin-independent [9]. However, in appendix A an example is given of a scattering process were the spin-dependent/independent description is not sufficient.

### 2.3.2 Indirect detection

In indirect detection experiments one tries to observe the radiation produced in dark matter annihilations. Since the radiation flux is proportional to the dark matter density squared it is natural to look at places with high expected dark matter density [9],

$$\Gamma_A \propto \rho_{DM}^2 \tag{2.5}$$

where $\Gamma_A$ is the annihilation rate and $\rho_{DM}$ is the dark matter density where the annihilation occurs.

These regions with expected higher dark matter densities are often called amplifiers. The galactic centre could act as an amplifier, but also the earth and the sun when the dark matter particles loose energy due to scattering with nuclei in the interior of said objects. Measuring the radiation flux from such amplifiers would require neutrino detectors however, since light would not be able to escape their interiors [9].

With this technique it is then possible to put constraints on various dark matter models and potentially discover indications of particle dark matter [9].

# 3

# Theory

This section describe the dark matter-nucleus interaction that is expected to occur in a direct detection experiment. It includes a review of the effective theory used in the simulations and a subsection concerning the general properties of $P$ and $CP$ transformations. In addition, the constrained form of the effective theory is presented, when working under the assumption of scalar dark matter. The section ends with a short review of the simulated observable, i.e the event rate and its relation to the scattering cross section.

## 3.1 Preliminaries

In this subsection, the conventions used and some of the theoretical preliminaries are presented.

### 3.1.1 Unit and metric convention

In this thesis, the standard metric for quantum field theory applications in particle physics is used [35].

$$g^{\mu\nu} = g_{\mu\nu} = \begin{pmatrix} 1 & 0 & 0 & 0 \\ 0 & -1 & 0 & 0 \\ 0 & 0 & -1 & 0 \\ 0 & 0 & 0 & -1 \end{pmatrix} \tag{3.1}$$

The contraction of two four-vectors consequently becomes

$$A^{\mu}B_{\mu} = g^{\mu\nu}A_{\nu}B_{\mu} = A_0B_0 - A_jB_j, \quad j = 1, 2, 3. \tag{3.2}$$

Unless stated otherwise, natural units are used [39], where

$$\hbar = c = 1 \tag{3.3}$$

### 3.1.2 Non-relativistic limit of the Dirac equation

Spinors corresponding to spin-1/2 particles described in this thesis, is spinors that satisfy the free Dirac equation [35],

$$(i\partial\!\!\!/ - m)u_s = 0 \tag{3.4}$$

where $\not{\partial} \equiv \gamma^\mu \partial_\mu$ and $s = 1, 2$. In the non-relativistic limit, these spinors simplify as [13],

$$\begin{aligned} u_s(p) &= \begin{pmatrix} \sqrt{p^\mu \cdot \sigma_\mu} \xi^s \\ \sqrt{p^\mu \cdot \bar{\sigma}_\mu} \xi^s \end{pmatrix} = \frac{1}{\sqrt{2(p^0 + m)}} \begin{pmatrix} (p^\mu \sigma_\mu + m)\xi^s \\ (p^\mu \bar{\sigma}_\mu + m)\xi^s \end{pmatrix} \\ &= \frac{1}{\sqrt{4m}} \begin{pmatrix} (2m - \vec{p} \cdot \vec{\sigma})\xi^s \\ (2m + \vec{p} \cdot \vec{\sigma})\xi^s \end{pmatrix} + \mathcal{O}(\vec{p}^2). \end{aligned} \tag{3.5}$$

Where $p^\mu = (m, \vec{p})$, $\xi^s$ is a two component spinor and

$$\sigma^\mu = (\mathbf{1}, \vec{\sigma}), \quad \bar{\sigma}^\mu = (\mathbf{1}, -\vec{\sigma}). \tag{3.6}$$

Here $\vec{\sigma}$ are simply the Pauli matrices [38, 39].

$$\sigma^1 = \begin{pmatrix} 0 & 1 \\ 1 & 0 \end{pmatrix}, \quad \sigma^2 = \begin{pmatrix} 0 & -i \\ i & 0 \end{pmatrix}, \quad \sigma^3 = \begin{pmatrix} 1 & 0 \\ 0 & -1 \end{pmatrix}. \tag{3.7}$$

Chiral bases are used for the Dirac matrices $\{\gamma^\mu, \gamma^\nu\} = 2g^{\mu\nu}$ [39].

$$\gamma^\mu = \begin{pmatrix} 0 & \sigma^\mu \\ \bar{\sigma}^\mu & 0 \end{pmatrix}, \quad \gamma^5 = \begin{pmatrix} -1 & 0 \\ 0 & 1 \end{pmatrix} \tag{3.8}$$

### 3.1.3 Scalar particles

A scalar particle could be described as quantum fluctuations that satisfy the Klein-Gordon equation [39].

$$(\Box + m^2)\Phi = 0 \tag{3.9}$$

Where $\Box = \partial^\mu \partial_\mu$ and $\Phi$ is scalar field [35]. It is indeed true that all scalar particles, composite or fundamental satisfy the Klein-Gordon equation. However since all free fields satisfy this equation as well, we will simply define scalar particles as particles that have spin-0 [39]. This in turn simply means that the effective operators introduced in section 3.3 which have a dark matter spin dependency will become 0.

## 3.2 P and CP-transformation

At the core of this thesis lies the question whether a certain dark matter-nucleus interactions violates parity ($P$) and charge conjugation parity ($CP$) transformations. All observations made so far supports the statement that $CPT$-symmetry is a fundamental symmetry of nature, where $T$ stands for time-reversal. In the Feynman–Stueckelberg interpretation, this is the same as Lorentz invariance [35, 39].

We do know however that there is room for violation of $CP$, correspondingly $T$-violation. In rare neutral kaon decay modes, $CP$-violation has been observed [15]. We also know that the weak interaction violates $C$, $P$, as well as $CP$ [39]. Since we do know that there is room for violations of $P$ and $CP$ in nature, it is then of interests to study how dark matter-nucleus interactions transforms under these transformations. In order to do this, it important to state what these transformations entail.

### 3.2.1 Parity

If we consider a single particle, the operator $P$ mirrors the particle in question, without changing its spin, i.e the sign of the momentum changes. As an example, this unitary operator $P$ transforms the state $a^s_{\boldsymbol{p}} |0\rangle$ to $a^s_{-\boldsymbol{p}} |0\rangle$. If this transformation is implemented on a Dirac field $\Psi(x)$ it can be written as in (3.10), [39].

$$P\Psi(x)P = \int \frac{d^3p}{(2\pi)^3} \frac{1}{\sqrt{2E_P}} \sum_s \left( \eta_a a^s_{-\boldsymbol{p}} u^s(p) e^{-ipx} + \eta_b^* b^{s\dagger}_{-\boldsymbol{p}} v^s(p) e^{ipx} \right) \tag{3.10}$$

Where $\eta_a$ and $\eta_b$ are phases that constrain the transformation so that $P$ returns the original observables, $b^{s\dagger}_{-\boldsymbol{p}}$ and $a^s_{-\boldsymbol{p}}$ are creation and annihilation operators, $u^s(p)$ and $v^s(p)$ are solutions to the Dirac equation, and $E_P$ is the energy.

With a change of variables $\tilde{p} = (p^0, -\boldsymbol{p})$ so that $p \cdot x = \tilde{p} \cdot (t, -\boldsymbol{x})$, $\tilde{p} \cdot \sigma = p \cdot \bar{\sigma}$ and $\tilde{p} \cdot \bar{\sigma} = p \cdot \sigma$, it is possible to write the solutions to the Dirac equation as

$$\begin{aligned} u(p) &= \gamma^0 u(\tilde{p}) \\ v(p) &= -\gamma^0 v(\tilde{p}). \end{aligned} \tag{3.11}$$

By implementing this in eq. (3.10) the parity transformation takes the form of

$$P\Psi(t, \boldsymbol{x})P = \eta_a \gamma^0 \Psi(t, -\boldsymbol{x}) \tag{3.12}$$

if the phases $\eta_b^* = -\eta_a$ [39]. This holds in the non-relativistic limit as well, something that can be seen by looking at (3.5).

$$\begin{aligned} u^s(p) &= \frac{1}{\sqrt{2(p^0 + m)}} \begin{pmatrix} (p^\mu \sigma_\mu + m)\xi^s \\ (p^\mu \bar{\sigma}_\mu + m)\xi^s \end{pmatrix} \\ &= \frac{1}{\sqrt{2(p^0 + m)}} \begin{pmatrix} (\tilde{p}^\mu \bar{\sigma}_\mu + m)\xi^s \\ (\tilde{p}^\mu \sigma_\mu + m)\xi^s \end{pmatrix} \\ &= \frac{1}{\sqrt{4m}} \begin{pmatrix} (2m - \boldsymbol{p} \cdot \vec{\sigma})\xi^s \\ (2m + \boldsymbol{p} \cdot \vec{\sigma})\xi^s \end{pmatrix} + \mathcal{O}(\boldsymbol{p}^2) \to \gamma^0 u^s_{\text{non-rel}}(\tilde{p}) \end{aligned} \tag{3.13}$$

From this it is then possible to see how different bilinears transform. For example the scalar bilinear $\bar{\Psi}(x)\Psi(x)$ [39].

$$P\bar{\Psi}\Psi P = |\eta_a|^2 \bar{\Psi}(t, -\boldsymbol{x})\gamma^0\gamma^0\Psi(t, -\boldsymbol{x}) = +\bar{\Psi}(t, -\boldsymbol{x})\Psi(t, -\boldsymbol{x}) \tag{3.14}$$

### 3.2.2 Charge Conjugation

Charge conjugation $C$ (sometimes written as † in the thesis) is the operator that transforms a particle into the corresponding anti-particle, but with the same spin. Thus the transformation is defined as below [39].

$$Ca^s_{\boldsymbol{p}}C = b^s_{\boldsymbol{p}}, \quad Cb^s_{\boldsymbol{p}}C = a^s_{\boldsymbol{p}} \tag{3.15}$$

The relation between $u^s(p)$ and $v^s(p)$ is given by eq. (3.16) and is simply derived from the complex conjugation of $v^s(p)$ with the definition $\xi^{-s} = -i\sigma^2(\xi^s)^*$ [39],

$$u^s(p) = -i\gamma^2(v^s(p))^*, \quad v^s(p) = -i\gamma^2(u^s(p))^* \tag{3.16}$$

Acting upon $\Psi(x)$ then yields

$$\begin{aligned} C\Psi(x)C &= \int \frac{d^3p}{(2\pi)^3}\frac{1}{\sqrt{2E_P}}\sum_s \Big( -i\gamma^2 b^s_{\boldsymbol{p}}(v^s(p))^* e^{-ipx} - i\gamma^2 a^{s\dagger}_{\boldsymbol{p}}(u^s(p))^* e^{ipx}\Big) \\ &= -i\gamma^2\Psi(x)^* = -i\gamma^2(\Psi^\dagger)^T = -i(\bar{\Psi}\gamma^0\gamma^0)^T. \end{aligned} \tag{3.17}$$

Similarly acting upon $\bar{\Psi}$ gives eq. (3.18) [39].

$$C\bar{\Psi}C = (-i\gamma^0\gamma^2\Psi)^T \tag{3.18}$$

As in the case of parity it is now possible to compute different fermionic bilinears from this. The same example of the scalar bilinear $\bar{\Psi}\Psi$ is given here [39],

$$C\bar{\Psi}\Psi(x)C = -i(\bar{\Psi}\gamma^0\gamma^0)^T(-i\gamma^0\gamma^2\Psi)^T = -\bar{\Psi}\gamma^2\gamma^0\gamma^0\gamma^2\Psi = +\bar{\Psi}\Psi \tag{3.19}$$

### 3.2.3 CP and Time reversal

Since the working assumption is that $CPT$ is a fundamental symmetry of nature, the product of the combined transformation of $CP$ and time reversal $T$ has to be +1. Thus $CP$ and $T$ should yield the same result. As an example, we know that the scalar bilinear $\bar{\Psi}\Psi$ is invariant under both $C$ and $P$, thus it is even under $CP$ as well. Consequently, it is also even under $T$.

## 3.3 Effective theory of dark matter direct detection

This section describes the effective theory used in order to model the dark matter-nucleus interactions simulated in this project. This effective theory describes all possible non-relativistic dark matter-nucleus interactions that are compatible with Galilean invariance and momentum conservation, not only the leading order interactions. This includes momentum- and velocity dependent operators in addition to the spin operators. An example of a model that includes these additional operators is given in appendix A. With this effective theory approach it is then possible to identify the nuclear response for each interactions corresponding to a specific target and dark matter mass $m$ [26].

**Non-relativistic limit of dark matter-nucleus interactions**

In the context of direct detection experiments we are interested in elastic scattering between dark matter particles and nucleons bound in nuclei. Thus all operators will be written as four-field operators in the following form

$$\mathcal{L}_{int} = \chi^+\mathcal{O}_\chi\chi^- N^+\mathcal{O}_N N^- \equiv \mathcal{O}\chi^+\chi^- N^+ N^- \tag{3.20}$$

Where $\mathcal{L}_{int}$ is the dark matter-nucleon interacting Lagrangian, $\chi$ and $N$ are the effective dark matter and nucleon fields, and $\mathcal{O}$ is an effective operator [26].

In constructing the full set of dark matter-nucleon interaction operators we will need to consider all constraints that apply to dark matter-nuclei interactions in the non-relativistic limit. In this limit, one of the most important symmetries that will act as a constraint is Galilean invariance. This means that the interacting Lagrangian is invariant under a constant shift of particle velocities, i.e the following transformation holds

$$\boldsymbol{T}_{Galilean}(\{t, \boldsymbol{x}\} \to \{t, \boldsymbol{x} + \boldsymbol{v}t\}) : \mathcal{L}_{int} \to \mathcal{L}_{int} \tag{3.21}$$

where $\boldsymbol{T}_{Galilean}(\{t, \boldsymbol{x}\} \to \{t, \boldsymbol{x} + \boldsymbol{v}t\})$ is simply a Galilean transformation shifting particle velocities and $v$ is the velocity [5, 26].

This implies that the dark matter-nucleon scattering amplitude can depend on the momentum transfer $q = k - k' = p' - p$ and obeys Galilean invariance by construction, with the Galilean invariant contribution $p$ and $k$. Thus there are only two independent momenta in a non-relativistic dark matter-nucleon interaction. In addition to the momentum transfer, the relative velocity is also invariant under $\boldsymbol{T}_{Galilean}$ [26].

$$\boldsymbol{T}_{Galilean} : \left[\vec{v} \equiv \vec{v}_{\chi,\text{in}} - \vec{v}_{N,\text{in}}\right] \to \vec{v} \tag{3.22}$$

The last constraint on the kinematics is energy conservation. In the center-of-mass frame the total kinetic energy is

$$E = \frac{1}{2}\mu_N v_{rel}^2 \tag{3.23}$$

where $\mu_N = \frac{m_N m_\chi}{m_N + m_\chi}$ is the reduced mass of the dark matter-nucleon system and $v_{rel} = v_\chi - v_N$. Where $v_\chi$ is the dark matter velocity and $v_N$ is the nucleon velocity. With initial and final energy being

$$\begin{aligned} E_{in} &= \frac{1}{2}\mu_N v^2 \\ E_{final} &= \frac{1}{2}\mu_N \left(\vec{v} + \frac{\vec{q}}{\mu_N}\right)^2 \end{aligned} \tag{3.24}$$

Thus by imposing energy conservation we have [26],

$$\vec{v} \cdot \vec{q} = -\frac{q^2}{2\mu_N}. \tag{3.25}$$

Another constraint is the hermaticity of the interaction, i.e the operators need to be self-adjoint. Taking the Hermitian conjugate of the interaction is the same as exchanging incoming and outgoing particles. This means that the momentum transfer $\vec{q}$ is anti-Hermitian. Thus we will use the Hermitian operator $i\vec{q}$ instead. Note that under Hermitian conjugation, $\vec{v}$ does not have definite parity [26],

$$\vec{v} \xrightarrow{\dagger} \vec{v}_{\chi,\text{out}} - \vec{v}_{N,\text{out}} = \vec{v} + \frac{\vec{q}}{\mu_N}. \tag{3.26}$$

By constructing a similar operator that satisfies $\vec{v}^{\perp} \cdot \vec{q} = 0$ we have a Hermitian operator [26],

$$\vec{v}^{\perp} \equiv \vec{v} + \frac{\vec{q}}{2\mu_N}. \tag{3.27}$$

Which we use together with $i\vec{q}$ to build dark matter-nucleon scattering amplitudes.

The last thing that needs to be included is particle spins. This consequently means that the four-field operators in eq. (3.20) can include $\gamma$ matrices. By treating the different possible spins of the dark matter particle in an unified way, we can write the spin-operators as $\vec{S}_\chi$ and $\vec{S}_N$ [26]. Thus if the dark matter particle is a spin-1/2 fermion, the spin-operator $\frac{1}{2}\vec{\sigma}$ will simple consist of the Pauli matrices [13, 38]. These will then act upon $\chi$ or $N$ spinors [26].

If the dark matter particle is a vector particle, then the effective spin operator is a spin-1 representation of the angular momentum generators $J^i$, which acts upon $\chi$. For a scalar dark matter particle, the operator is simply not present. All of these above mentioned operators are invariant under Hermitian conjugation, thus we have a set of operators from which the effective dark matter-nucleon interaction operators can be constructed [26].

It is convenient to categorise the possible operators in terms of their properties under $P$ and $C$. One reason for this is because of the constraints concerning $CPT$ symmetry. Since this effective theory is ultimately expected to be integrated in a Lorentz invariant field theory, it needs to be even under $CPT$, which for a $CP$-symmetric theory means $T$-symmetry (see section 3.2). Spins acts like angular momentum, therefore it will be odd under $T$, but even under $P$. All velocities change sign under $T$, and both $\vec{q}$ and $\vec{v}^{\perp}$ are odd under $P$. This yields the following transformation table for the Hermitian invariant operators [26].

Table 3.1: Table of Hermitian invariants under † ($C$), $T$ and $P$ [26].

| | † | $T$ | $P$ |
|---|---|---|---|
| $\vec{S}$ | $+1$ | $-1$ | $+1$ |
| $i\vec{q}$ | $+1$ | $+1$ | $-1$ |
| $\vec{v}^{\perp}$ | $+1$ | $-1$ | $-1$ |

Since the momentum transfer squared $q^2/m_n^2$, where $m_n$ is the nucleon mass, is an invariant scalar that only depends on the dark matter kinematics, all allowed operators $\mathcal{O}$ can be expanded with this quantity and still be allowed. Furthermore, the operators $\mathcal{O}$ can be expanded in powers of $v^{\perp}$. At second order in $\vec{q}$ and of first order in $v^{\perp}$ the effective operators allowed within this framework are given in table 3.2. The effective interacting Lagrangian density is then given by eq. (3.28) [26],

$$\mathcal{L}_{int}^{Eff} = \sum_{N=n,P} \sum_i c_i^{(N)} \mathcal{O}_i \chi^+ \chi^- N^+ N^-. \tag{3.28}$$

Table 3.2: Table over possible effective operators in the non-relativistic limit with spin-1 and spin-0 mediators classified with respect to their properties under $C$, $P$ and $T$, such that $CPT = +1$ [26]. Note that $\mathcal{O}_2$ is of higher in $v^{\perp}$. This operator will be neglected in further calculations.

| | $\dagger$ | $P$ | $T$ |
|---|---|---|---|
| $\mathcal{O}_1 = \mathbb{1}$ | $+1$ | $+1$ | $+1$ |
| $\mathcal{O}_2 = (\vec{v}^{\perp})^2$ | $+1$ | $+1$ | $+1$ |
| $\mathcal{O}_3 = i\vec{S}_N \cdot (\vec{q} \times \vec{v}^{\perp})$ | $+1$ | $+1$ | $+1$ |
| $\mathcal{O}_4 = \vec{S}_\chi \cdot \vec{S}_N$ | $+1$ | $+1$ | $+1$ |
| $\mathcal{O}_5 = i\vec{S}_\chi \cdot (\vec{q} \times \vec{v}^{\perp})$ | $+1$ | $+1$ | $+1$ |
| $\mathcal{O}_6 = (\vec{S}_\chi \cdot \vec{q})(\vec{S}_N \cdot \vec{q})$ | $+1$ | $+1$ | $+1$ |
| $\mathcal{O}_7 = \vec{S}_N \cdot \vec{v}^{\perp}$ | $-1$ | $-1$ | $+1$ |
| $\mathcal{O}_8 = \vec{S}_\chi \cdot \vec{v}^{\perp}$ | $-1$ | $-1$ | $+1$ |
| $\mathcal{O}_9 = i\vec{S}_\chi \cdot (\vec{S}_N \times \vec{q})$ | $-1$ | $-1$ | $+1$ |
| $\mathcal{O}_{10} = i\vec{S}_N \cdot \vec{q}$ | $+1$ | $-1$ | $-1$ |
| $\mathcal{O}_{11} = i\vec{S}_\chi \cdot \vec{q}$ | $+1$ | $-1$ | $-1$ |

Our effective field theory approach with constant coupling coefficients is valid as long as: 1) $\frac{|\vec{q}|}{m_n} \ll 1$; 2) $q^2 \ll M^2$, where $M$ is the mass of the particle that mediates the interaction between dark matter and nucleons.

Since the recoil energy is the measured quantity in direct detection experiments, it is useful to have this limit in terms of $E_R$. In elastic scattering the relation between the recoil energy and momentum transfer is given by eq. (3.29) [26],

$$q = \sqrt{2m_T E_R}. \tag{3.29}$$

The minimum dark matter velocity that can cause nuclear recoil is given by $v_{min} = \sqrt{(m_T E_R)/(2\mu_N^2)}$ [12]. Since the cut-off of the Maxwell-Boltzmann distribution is believed to be around 544 km/s $\approx 2 \cdot 10^{-3}$ [Natural units], the maximum momentum transfer of the effective theory is around $q_{max} \approx 400$ MeV. The distribution is thought to drop drastically around $v \approx 10^{-3}$ so the momentum transfer will rarely exceed $q \approx 200$ MeV. This corresponds to a recoil energy of $E_{R,max} \approx 200$ keV. Consequently this also means that the mediator mass scale needs to fulfil the following inequality [26].

$$M \geq \text{constant} \cdot 200 \text{ MeV} \tag{3.30}$$

### Nuclear response

Having developed an effective theory for dark matter-nucleon interactions, we now have to find the response of nuclei to such interactions. In order to classify their response functions we first start with the now established interaction Lagrangian

[26],

$$\begin{aligned}\mathcal{L}_{int}^{Eff} &= c_1\mathbb{1} + c_2\vec{v}^{\perp}\cdot\vec{v}^{\perp} + c_3\vec{S}_N\cdot(\vec{q}\times\vec{v}^{\perp}) + c_4\vec{S}_\chi\cdot\vec{S}_N \\ &+ic_5\vec{S}_\chi\cdot(\vec{q}\times\vec{v}^{\perp}) + c_6\vec{S}_\chi\cdot\vec{q}\vec{S}_N\cdot\vec{q} + c_7\vec{S}_N\cdot\vec{v}^{\perp} \\ &+c_8\vec{S}_\chi\cdot\vec{v}^{\perp} + ic_9\vec{S}_\chi\cdot(\vec{S}_N\times\vec{q}) + ic_{10}\vec{S}_N\cdot\vec{q} + ic_{11}\vec{S}_\chi\cdot\vec{q}.\end{aligned} \tag{3.31}$$

Here, $c_i$ is now written in isospin space $c_i = c_i^0\mathbf{1} + c_i^1\tau_3$ where the operators, state vector and couplings are given below [36],

$$\begin{aligned} c_i^0 &= \frac{1}{2}(c_i^P + c_i^n), \quad c_i^1\frac{1}{2}(c_i^P - c_i^n) \\ \mathbf{1} &= \begin{pmatrix}1 & 0\\ 0 & 1\end{pmatrix}, \quad \tau_3 = \begin{pmatrix}1 & 0\\ 0 & -1\end{pmatrix} \\ |P\rangle &= \begin{pmatrix}1\\0\end{pmatrix}, \quad |n\rangle = \begin{pmatrix}0\\1\end{pmatrix}.\end{aligned} \tag{3.32}$$

By separating the Hermitian velocity into one part that acts coherently on the center-of-mass velocity, and one part part that acts only on the separation distance in between the nucleons, $\vec{v}^{\perp} = \vec{v}_T^{\perp} + \vec{v}_N^{\perp}$, where the two velocities are given in eq. (3.33) [26],

$$\begin{aligned}\vec{v}_T^{\perp} &= \vec{v}_T + \frac{\vec{q}}{2\mu_T} \\ \vec{v}_N^{\perp} &= -\frac{1}{2}(\vec{v}_{N,in} - \vec{v}_{N,out}).\end{aligned} \tag{3.33}$$

The reason for the above separation is that $\vec{v}_T^{\perp}$ depends on the scattering process and $\vec{v}_N^{\perp}$ depends on the structure of the nucleus. This will in turn allow us to find nuclear response functions that are independent of the dark matter input [26]. From eq. (3.31) it can now be seen that we can create nuclear "charges" $\mathbb{1}$, $\vec{v}_N^{\perp}\cdot\vec{v}_N^{\perp}$ and $\vec{S}_N\cdot\vec{v}_N^{\perp}$. These transform under $P$ and $T$ as even-even, even-even and odd-even. In addition, the nuclear "currents" $\vec{S}_N$, $\vec{v}_N^{\perp}$ and $\vec{S}_N\times\vec{v}_N^{\perp}$ also arise from eq. (3.31) which transforms under $P$ and $T$ as odd-odd, even-odd and odd-even. This reveals that there are six independent nuclear response functions under the assumption of a nuclear ground state with good $P$ and $CP$, i.e even-even under both $P$ and $CP$ [26].

In order to construct these response functions the common nuclear physics assumption of $\vec{S}_N$ and $\vec{v}_N^{\perp}$ acting upon individual nucleons is made. We can now write an effective Lagrangian where the nuclear part is separated from the scattering kinematics and the dark matter input [26].

$$\begin{aligned}\mathcal{L}_{int}^{Eff} &= l_0\mathbb{1} + l_0^A[-2\vec{v}_N^{\perp}\cdot\vec{S}_N] + \vec{l}_5\cdot[2\vec{S}_N] \\ &+\vec{l}_M[-\vec{v}_N^{\perp}] + \vec{l}_E\cdot[2i\vec{v}_N^{\perp}\times\vec{S}_N] \\ &= l_0\mathbb{1} + l_0^A\Big(\frac{\vec{p}_i+\vec{p}_f}{2m_N}\Big)\cdot\vec{\sigma} + \vec{l}_5\cdot\vec{\sigma} \\ &+\vec{l}_M\cdot\Big(\frac{\vec{p}_i+\vec{p}_f}{2m_N}\Big) + \vec{l}_E\cdot\Big(-i\frac{\vec{p}_i+\vec{p}_f}{2m_N}\times\vec{\sigma}\Big)\end{aligned} \tag{3.34}$$

where the coefficients $l_i$ are given in the table below. The operator $\mathcal{O}_2 = (\vec{v}^{\perp})^2$ have been ignored in this table. This is mainly due to that this interaction belongs to $\boldsymbol{\mathcal{O}}(v^2/c^2)$ and will massively be suppressed with respect to $\mathcal{O}_1 \in \boldsymbol{\mathcal{O}}(v^0/c^0)$ that behaves the same under $C$ and $P$ [26].

Table 3.3: Table of coefficients containing the dark matter input and scattering kinematics [26, 36].

| $l_i$ | Type: |
|---|---|
| $l_0 = c_1 - i(\vec{q} \times \vec{S}_\chi) \cdot \vec{v}_T^{\perp} c_5 + \vec{S}_\chi \cdot \vec{v}_T^{\perp} c_8 + i\vec{q} \cdot \vec{S}_\chi c_{11}$ | Charge |
| $l_0^A = -\frac{1}{2} c_7$ | Axial charge |
| $\vec{l}_5 = \frac{1}{2}\Big[i\vec{q} \times \vec{v}_T^{\perp} c_3 + \vec{S}_\chi c_4 + (\vec{S}_\chi \cdot \vec{q})\vec{q} c_6 + \vec{v}_T^{\perp} c_7 + i\vec{q} \times \vec{S}_\chi c_9 + i\vec{q} c_{10}\Big]$ | Axial vector |
| $\vec{l}_M = i\vec{q} \times \vec{S}_\chi c_5 - \vec{S}_\chi c_8$ | Vector magnetic |
| $\vec{l}_E = \frac{1}{2}\vec{q} c_3$ | Vector electric |

The Hamiltonian for dark matter-nucleon interactions can be determined by applying the following transformation to coordinate space to eq. (3.34),

$$\frac{\vec{p}_i + \vec{p}_f}{2m_N} \rightarrow \frac{1}{2m_N}\Big( -\frac{1}{i}\overleftarrow{\nabla}\delta(\vec{x} - \vec{x}_i) + \delta(\vec{x} - \vec{x}_i)\frac{1}{i}\overrightarrow{\nabla}\Big) \tag{3.35}$$

and summing over the nucleons $A$. The corresponding Hamiltonian density is then given by eq. (3.36) [26],

$$\begin{aligned}
\mathcal{H}^{Eff}(\vec{x}) &= \sum_{i=1}^{A} l_0(i)\delta(\vec{x} - \vec{x}_i) + \sum_{i=1}^{A} \vec{l}_5(i) \cdot \vec{\sigma}(i)\delta(\vec{x} - \vec{x}_i) \\
&+ \sum_{i=1}^{A} l_0^A(i)\frac{1}{2m_N}\Big[ -\frac{1}{i}\overleftarrow{\nabla}_i \cdot \vec{\sigma}(i)\delta(\vec{x} - \vec{x}_i) + \delta(\vec{x} - \vec{x}_i)\vec{\sigma}(i) \cdot \frac{1}{i}\overrightarrow{\nabla}_i\Big] \\
&+ \sum_{i=1}^{A} \vec{l}_M(i) \cdot \frac{1}{2m_N}\Big[ -\frac{1}{i}\overleftarrow{\nabla}_i\delta(\vec{x} - \vec{x}_i) + \delta(\vec{x} - \vec{x}_i)\frac{1}{i}\overrightarrow{\nabla}_i\Big] \\
&+ \sum_{i=1}^{A} \vec{l}_E(i) \cdot \frac{1}{2m_N}\Big[\overleftarrow{\nabla}_i \times \vec{\sigma}(i)\delta(\vec{x} - \vec{x}_i) + \delta(\vec{x} - \vec{x}_i)\vec{\sigma}(i) \times \overrightarrow{\nabla}_i\Big].
\end{aligned} \tag{3.36}$$

This effective Hamiltonian density can then be expanded with the use of spherical harmonics and Bessel functions. [26],

$$\begin{aligned}
e^{i\vec{q}\cdot\vec{x}_i} &= \sum_{J=0}^{\infty} \sqrt{4\pi}[J]i^J j_J(qx_i)Y_{J0}(\Omega_{x_i}) \\
\hat{e}_\lambda e^{i\vec{q}\cdot\vec{x}_i} &= \begin{cases} \sum_{J=0}^{\infty} \sqrt{4\pi}[J]i^{J-1} j_J(qx_i)Y_{J0}(\Omega_{x_i}), & \lambda = 0 \\ \\ \sum_{J\geq 1}^{\infty} \sqrt{2\pi}[J]i^{J-2}\Big[\lambda j_J(qx_i)\vec{Y}^{\lambda}_{JJ1}(\Omega_{x_i}) + \frac{\vec{\nabla}_i}{q} \times j_J(qx_i)\vec{Y}^{\lambda}_{JJ1}(\Omega_{x_i})\Big], & \lambda \pm 1 \end{cases}
\end{aligned} \tag{3.37}$$

Where $e^{i\vec{q}\cdot\vec{x}_i}$ is the spherical harmonic plane wave expansion for scalar nuclear charges and $\hat{e}_\lambda e^{i\vec{q}\cdot\vec{x}_i}$ is the expansion of vector nuclear currents in terms of vector spherical harmonics. Here, $[J] \equiv \sqrt{2J+1}$ and $\hat{e}_\lambda$, $\lambda = -1, 0, 1$ are spherical unit vectors defined with $z$-axis along $\hat{q} = \vec{q}/q$. Since the Hamiltonian has the form

$$\int d\vec{x} e^{-i\vec{q}\cdot\vec{x}} \Big[ l_0 \langle J_i M_i | \hat{\rho}(\vec{x}) | J_i M_i \rangle - \vec{l} \cdot \langle J_i M_i | \hat{\vec{j}}(\vec{x}) | J_i M_i \rangle \Big] \tag{3.38}$$

the transition matrix element is given by eq. (3.39) in terms of standard nuclear operators for weak interactions [22, 26, 36, 43],

$$\begin{aligned}
&\langle j_\chi, M_{\chi f}; j_N M_{Nf} | \Bigg[ \sum_{J=0}^{\infty} \sqrt{4\pi(2J+1)} (-i)^J \Big[ l_0 M_{J0}(q) - i l_0^A \frac{q}{m_N} \tilde{\Omega}_{q0}(q) \Big] \\
&+ \sum_{J=1}^{\infty} \sqrt{2\pi(2J+1)} (-i)^J \sum_{\lambda=\pm 1} (-1)^\lambda \Big[ \vec{l}_{5\lambda} \Big( \lambda \Sigma_{J-\lambda}(q) + i \Sigma'_{J-\lambda}(q) \Big) \\
&- i \frac{q}{m_N} \vec{l}_{M\lambda} \Big( \lambda \Delta_{J-\lambda}(q) + i \Delta'_{J-\lambda}(q) \Big) - i \frac{q}{m_N} \vec{l}_{E\lambda} \Big( \lambda \tilde{\Phi}_{J-\lambda}(q) + i \tilde{\Phi}'_{J-\lambda}(q) \Big) \Big] \\
&+ \sum_{J=0}^{\infty} \sqrt{4\pi(2J+1)} (-i)^J \Big[ i \vec{l}_{50} \Sigma''_{J0}(q) + \frac{q}{m_N} \vec{l}_{M0} \tilde{\Delta}''_{J0}(q) \\
&+ \frac{q}{m_N} \vec{l}_{E0} \Phi''_{J0}(q) \Big] \Bigg] | j_\chi, M_{\chi i}; j_N M_{Ni} \rangle
\end{aligned} \tag{3.39}$$

where the nucleon operators are defined as $O_{JM}(q) \equiv \sum_{i=1}^{A} O_{JM}(q\vec{x}_i)$. By assuming that the nuclear ground state is an approximate eigenstate of $P$ and $CP$ and by the fact that we are interested in the amplitude squared we can simplify the above expression by looking at the nuclear operators behaviour under $P$ and $CP$ [36].

Table 3.4: Table of nuclear operators and how they transform under $P$ and $CP$ [36].

| Projection | Charge/Current | Operator | Even $J$ | Odd $J$ |
|---|---|---|---|---|
| Charge | Vector charge | $M_{JM}$ | E-E | O-O |
| Charge | Axial-vector charge | $\tilde{\Omega}_{JM}$ | O-E | E-O |
| Longitudinal | Spin current | $\Sigma''_{JM}$ | O-O | E-E |
| Transverse magnetic | $-\vert\vert-$ | $\Sigma_{JM}$ | E-O | O-E |
| Transverse electric | $-\vert\vert-$ | $\Sigma'_{JM}$ | O-O | E-E |
| Longitudinal | Convection current | $\tilde{\Delta}''_{JM}$ | E-O | O-E |
| Transverse magnetic | $-\vert\vert-$ | $\Delta_{JM}$ | O-O | E-E |
| Transverse electric | $-\vert\vert-$ | $\Delta'_{JM}$ | E-O | O-E |
| Longitudinal | Spin-velocity current | $\Phi''_{JM}$ | E-E | O-O |
| Transverse magnetic | $-\vert\vert-$ | $\tilde{\Phi}_{JM}$ | O-E | E-O |
| Transverse electric | $-\vert\vert-$ | $\tilde{\Phi}'_{JM}$ | E-E | O-O |

$$
\begin{aligned}
&\langle j_\chi, M_{\chi f}; j_N M_{Nf}| \Bigg[ \sum_{J=0,2..}^{\infty} \sqrt{4\pi(2J+1)}(-i)^J \Big[ l_0 M_{J0}(q) + \frac{q}{m_N} \vec{l}_{E0} \Phi''_{J0}(q) \Big] \\
&+ \sum_{J=1,3...}^{\infty} \sqrt{2\pi(2J+1)}(-i)^J \sum_{\lambda \pm 1} (-1)^\lambda \Big[ i\vec{l}_{5\lambda} \Sigma'_{J-\lambda} - i\frac{q}{mN} \vec{l}_{m\lambda} \lambda \Delta_{J-\lambda}(q) \Big] \\
&+ \sum_{J=2,4,..}^{\infty} \sqrt{2\pi(2J+1)}(-i)^J \sum_{\lambda \pm 1} \Big[ \frac{q}{m_N} \vec{l}_{E\lambda} \tilde{\Phi}'_{J-\lambda}(q) \\
&+ \sum_{J=1,3,...}^{\infty} \sqrt{4\pi(2J+1)}(-i)^J \Big[ i\vec{l}_{50} \Sigma''_{J0}(q) \Big] \Bigg] |j_\chi, M_{\chi i}; j_N M_{Ni}\rangle
\end{aligned}
\tag{3.40}
$$

Averaging over initial nuclear spins and summing over final nuclear spins then yields the amplitude squared given in eq. (3.41) [26, 36].

$$
\begin{aligned}
&\overline{|\mathcal{M}|^2}^{\text{elastic}}_{\text{nucleus}/Eff} = \frac{4\pi}{2J_i+1} \Bigg\{ \sum_{J=1,3,...}^{\infty} |\langle J_N || \vec{l}_5 \cdot \hat{q} \Sigma''_J(q) || J_N \rangle|^2 \\
&+ \sum_{J=0,2,...}^{\infty} \Big[ |\langle J_N || l_0 M_J(q) || J_N \rangle|^2 + |\langle J_N || \vec{l}_E \cdot \hat{q} \frac{q}{m_N} \Phi''_J(q) || J_N \rangle|^2 \\
&+ 2\mathrm{Re}\Big( \langle J_N || \vec{l}_E \cdot \hat{q} \frac{q}{m_N} \Phi''_J(q) || J_N \rangle \langle J_N || l_0 M_J(q) || J_N \rangle^* \Big) \Big] \\
&+ \frac{q^2}{2m_N^2} \sum_{J=2,4,...}^{\infty} \Big( \langle J_N || \vec{l}_E \tilde{\Phi}'_J(q) || J_N \rangle \cdot \langle J_N || \vec{l}_E \tilde{\Phi}'_J(q) || J_N \rangle^* - |\langle J_N || \vec{l}_E \tilde{\Phi}'_J(q) || J_N \rangle|^2 \Big) \\
&+ \sum_{J=1,3,...}^{\infty} \Bigg\{ \frac{q^2}{2m_N} \Big( \langle J_N || \vec{l}_M \Delta_J(q) || J_N \rangle \cdot \langle J_N || \vec{l}_M \Delta_J(q) || J_N \rangle^* - |\langle J_N || \vec{l}_M \cdot \Delta_J(q) || J_N \rangle|^2 \Big) \\
&+ \frac{1}{2} \Big( \langle J_N || \vec{l}_5 \Sigma'_J(q) || J_N \rangle \cdot \langle J_N || \vec{l}_5 \Sigma'_J(q) || J_N \rangle^* - |\langle J_N || \vec{l}_5 \Sigma'_J(q) || J_N \rangle|^2 \Big) \\
&+ 2\mathrm{Re}\Big( i\hat{q} \cdot \langle J_N || \vec{l}_M \frac{q}{m_N} \Delta_J(q) || J_N \rangle \times \langle J_N || \vec{l}_5 \Sigma'_J(q) || J_N \rangle^* \Big) \Bigg\} \Bigg\}
\end{aligned}
\tag{3.41}
$$

Where the nuclear operators are given by eq. (3.42) in terms of spherical Bessel functions $j_J(qx)$ and vector spherical harmonics $\vec{Y}_{JLM}$ [26],

$$
\begin{aligned}
&M_{JM} \equiv j_J(qx) Y_{JM}(\Omega_x)\\
&\vec{M}_{JLM} \equiv j_L(qx)\vec{Y}_{JLM}\\
&\Delta_{JM} \equiv \vec{M}_{MJJ}(q\vec{x}) \cdot \frac{1}{q}\vec{\nabla}\\
&\Sigma'_{JM} \equiv -i\Big\{\frac{1}{q}\vec{\nabla} \times \vec{M}_{MJJ}(q\vec{x})\Big\} \cdot \vec{\sigma} = [J]^{-1}\Big\{-\sqrt{J}\vec{M}_{MJJ+1}(q\vec{x}) + \sqrt{J+1}\vec{M}_{MJJ-1}(q\vec{x})\Big\} \cdot \vec{\sigma}\\
&\Sigma''_{JM} \equiv \Big\{\frac{1}{q}\vec{\nabla} M_{JM}(q\vec{x})\Big\} \cdot \vec{\sigma} = [J]^{-1}\Big\{\sqrt{J+1}\vec{M}_{MJJ+1}(q\vec{x}) + \sqrt{J}\vec{M}_{MJJ-1}(q\vec{x})\Big\} \cdot \vec{\sigma}\\
&\tilde{\Phi}'_{JM} \equiv \Big(\frac{1}{q}\vec{\nabla} \times \vec{M}_{MJJ}(q\vec{x})\Big) \cdot \Big(\vec{\sigma} \times \frac{1}{q}\vec{\nabla}\Big) + \frac{1}{2}\vec{M}_{MJJ}(q\vec{x}) \cdot \vec{\sigma}\\
&\Phi''_{JM} \equiv i\Big(\frac{1}{q}\vec{\nabla} M_{JM}(q\vec{x})\Big) \cdot \Big(\vec{\sigma} \times \frac{1}{q}\vec{\nabla}\Big).
\end{aligned}
\tag{3.42}
$$

Eq. (3.41) can be further simplified if all couplings behave the same in isospin. Then the isospin dependence $\mathbb{1} + \tau_3$ can be incorporated in to the single particle nuclear operators in eq. (3.42). Thus we have the final simplified expression for the amplitude squared [26],

$$
\begin{aligned}
\overline{|\mathcal{M}|^2}^{\text{elastic}}_{\text{nucleus}/Eff} = \frac{4\pi}{2J_i+1}\Bigg\{ &\sum_{J=1,3,\ldots}^{\infty} \vec{l}_5 \cdot \hat{q}\vec{l}^{\,*}_5 \cdot \hat{q} |\langle J_N || \Sigma''_J(q) || J_N \rangle|^2\\
+ &\sum_{J=0,2,\ldots}^{\infty} \Big[ l_0 l_0^* |\langle J_N || M_J(q) || J_N\rangle|^2 + \vec{l}_E \cdot \hat{q}\vec{l}^{\,*}_E \cdot \hat{q} |\langle J_N || \frac{q}{m_N}\Phi''_J(q) || J_N\rangle|^2\\
+ &2\mathrm{Re}\Big(\vec{l}_E \cdot \hat{q} l_0^* \langle J_N || \frac{q}{m_N}\Phi''_J(q) || J_N\rangle \langle J_N || M_J(q) || J_N\rangle^*\Big)\Big]\\
+ &\frac{q^2}{2m_N^2}\Big(\vec{l}_E \cdot \vec{l}^{\,*}_E - \vec{l}_E \cdot \hat{q}\vec{l}^{\,*}_E \cdot \hat{q}\Big) \sum_{J=2,4,\ldots}^{\infty} |\langle J_N || \tilde{\Phi}'_J(q) || J_N\rangle|^2\\
+ &\sum_{J=1,3,\ldots}^{\infty} \Big\{ \frac{q^2}{2m_N}\Big(\vec{l}_M \cdot \vec{l}^{\,*}_M - \vec{l}_M \cdot \hat{q}\vec{l}^{\,*}_M \cdot \hat{q}\Big) |\langle J_N || \Delta_J(q) || J_N\rangle|^2\\
+ &\frac{1}{2}\Big(\vec{l}_5 \cdot \vec{l}^{\,*}_5 - \vec{l}_5 \cdot \hat{q}\vec{l}^{\,*}_5 \cdot \hat{q}\Big) |\langle J_N || \Sigma'_J(q) || J_N\rangle|^2\\
+ &2\mathrm{Re}\Big[ i\hat{q} \cdot \Big(\vec{l}_M \times \vec{l}_5\Big) \langle J_N || \frac{q}{m_N}\Delta_J(q) || J_N\rangle \langle J_N || \Sigma'_J(q) || J_N\rangle^*\Big]\Big\}\Bigg\}.
\end{aligned}
\tag{3.43}
$$

Note that with this simplification the operator $\tilde{\Phi}'_{JM}$ does not contribute to the transition probability since $\vec{l}_E \cdot \vec{l}^{\,*}_E - \vec{l}_E \cdot \hat{q}\vec{l}^{\,*}_E \cdot \hat{q} = 0$. If the effective theory is extended to include more exotic mediators than spin-0 and spin-1 the corresponding response function will be non-zero [26, 36].

It is now possible to define the amplitude squared in terms of defined dark matter and nuclear response functions [36].

$$\overline{|\mathcal{M}|^2}^{\text{elastic}}_{\text{nucleus}/Eff} = \frac{4\pi}{2J_i+1}\Bigg\{\Bigg[R_M(\vec{v}_T^{\perp 2},\vec{q}^{\,2})W_M(y) + R_{\Sigma''}(\vec{v}_T^{\perp 2},\vec{q}^{\,2})W_{\Sigma''}(y) + R_{\Sigma'}(\vec{v}_T^{\perp 2},\vec{q}^{\,2})W_{\Sigma'}(y)\Bigg] + \frac{\vec{q}^{\,2}}{m_N^2}\Bigg[R_{\Phi''}(\vec{v}_T^{\perp 2},\vec{q}^{\,2})W_{\Phi''}(y) + R_{\Phi''M}(\vec{v}_T^{\perp 2},\vec{q}^{\,2})W_{\Phi''M}(y) + R_{\Delta}(\vec{v}_T^{\perp 2},\vec{q}^{\,2})W_{\Delta}(y) + R_{\Delta\Sigma'}(\vec{v}_T^{\perp 2},\vec{q}^{\,2})W_{\Delta\Sigma'}(y)\Bigg]\Bigg\} \tag{3.44}$$

The dark matter response functions are then given by eq. (3.45) and the nuclear response functions by eq. (3.46) [36],

$$\begin{aligned}
R_M(\vec{v}_T^{\perp 2},\vec{q}^{\,2}) &= c_1^2 + \frac{j_\chi(j_\chi+1)}{3}\Big[\vec{q}^{\,2}\vec{v}_T^{\perp 2}c_5^2 + \vec{q}^{\,2}\vec{v}^{\perp 2}c_8^2 + \vec{q}^{\,2}c_{11}^2\Big]\\
R_{\Phi''}(\vec{v}_T^{\perp 2},\vec{q}^{\,2}) &= \frac{1}{4}\vec{q}^{\,2}c_3^2\\
R_{\Phi''M}(\vec{v}_T^{\perp 2},\vec{q}^{\,2}) &= c_3c_1\\
R_{\Sigma''}(\vec{v}_T^{\perp 2},\vec{q}^{\,2}) &= \frac{1}{4}\vec{q}^{\,2}c_{10}^2 + \frac{j_\chi(j_\chi+1)}{12}\Big[c_4^2 + \vec{q}^{\,2}(c_4c_6 + c_6c_4) + \vec{q}^{\,4}c_6^2\Big]\\
R_{\Sigma'}(\vec{v}_T^{\perp 2},\vec{q}^{\,2}) &= \frac{1}{8}\Big[\vec{q}^{\,2}\vec{v}_T^{\perp 2}c_3^2 + \vec{v}_T^{\perp 2}c_7^2\Big] + \frac{j_\chi(j_\chi+1)}{12}\Big[c_4^2 + \vec{q}^{\,2}c_9^2\Big]\\
R_{\Delta}(\vec{v}_T^{\perp 2},\vec{q}^{\,2}) &= \frac{j_\chi(j_\chi+1)}{3}\Big[c_5^2 + c_8^2\Big]\\
R_{\Delta\Sigma'}(\vec{v}_T^{\perp 2},\vec{q}^{\,2}) &= \frac{j_\chi(j_\chi+1)}{3}\Big[c_5c_4 - c_8c_9\Big],
\end{aligned} \tag{3.45}$$

$$\begin{aligned}
W_M(y) &= \sum_{J=0,2,\ldots}^{\infty} \langle j_N||M_J(q)||j_N\rangle \langle j_N||M_J(q)||j_N\rangle\\
W_{\Sigma''}(y) &= \sum_{J=1,3,\ldots}^{\infty} \langle j_N||\Sigma''_J(q)||j_N\rangle \langle j_N||\Sigma''_J(q)||j_N\rangle\\
W_{\Sigma'}(y) &= \sum_{J=1,3,\ldots}^{\infty} \langle j_N||\Sigma'_J(q)||j_N\rangle \langle j_N||\Sigma'_J(q)||j_N\rangle\\
W_{\Phi''}(y) &= \sum_{J=0,2,\ldots}^{\infty} \langle j_N||\Phi''_J(q)||j_N\rangle \langle j_N||\Phi''_J(q)||j_N\rangle\\
W_{\Phi''M}(y) &= \sum_{J=0,2,\ldots}^{\infty} \langle j_N||\Phi''_J(q)||j_N\rangle \langle j_N||M_J(q)||j_N\rangle\\
W_{\Delta}(y) &= \sum_{J=1,3,\ldots}^{\infty} \langle j_N||\Delta_J(q)||j_N\rangle \langle j_N||\Delta_J(q)||j_N\rangle\\
W_{\Delta\Sigma'}(y) &= \sum_{J=1,3,\ldots}^{\infty} \langle j_N||\Delta_J(q)||j_N\rangle \langle j_N||\Sigma'_J(q)||j_N\rangle .
\end{aligned} \tag{3.46}$$

Equation (3.44) and the response functions (3.45), (3.46) are the primary expressions evaluated in the Mathematica package used in the simulations performed in this thesis, i.e *DMFormFactor* [36].

## 3.4 Scalar dark matter particles

This thesis aims to study the question whether the couplings of scalar dark matter particles that interacts with atomic nuclei is invariant under $P$ and $CP$. Since the dark matter in this context is assumed to have spin 0, the coupling coefficients of effective operators that are dependent on the dark matter spin $\vec{S}_\chi$ will be set to 0. The remaining operators classified with respect to $P$ and $CP$ are given in table 3.5.

Table 3.5: Table of scalar dark matter operators in the context of the effective field theory described in section 3.3. Note that $\mathcal{O}_2 = (\vec{v}^\perp)^2$ is not taken into consideration here since it would be massively suppressed with respect to $\mathcal{O}_1$ [26].

| Scalar operators | $P$ | $CP$ |
|---|---|---|
| $\mathcal{O}_1 = \mathbb{1}$ | $+1$ | $+1$ |
| $\mathcal{O}_3 = i\vec{S}_N \cdot (\vec{q} \times \vec{v}^\perp)$ | $+1$ | $+1$ |
| $\mathcal{O}_7 = \vec{S}_N \cdot \vec{v}^\perp$ | $-1$ | $+1$ |
| $\mathcal{O}_{10} = i\vec{S}_N \cdot \vec{q}$ | $-1$ | $-1$ |

With the constraints of spin-0 dark matter eq. (3.41) will be reduced to

$$\begin{aligned}
\overline{|\mathcal{M}|^2}^{\text{elastic}}_{\text{nucleus}/Eff} &= \frac{4\pi}{2J_i+1}\Bigg\{ \sum_{J=1,3,\ldots}^{\infty} |\langle J_N || \vec{l}_5 \cdot \hat{q}\Sigma''_J(q) || J_N\rangle|^2 \\
&+ \sum_{J=0,2,\ldots}^{\infty} \Big[ |\langle J_N || l_0 M_J(q) || J_N\rangle|^2 + |\langle J_N || \vec{l}_E \cdot \hat{q}\frac{q}{m_N}\Phi''_J(q) || J_N\rangle|^2 \\
&+ 2\mathrm{Re}\Big( \langle J_N || \vec{l}_E \cdot \hat{q}\frac{q}{m_N}\Phi''_J(q) || J_N\rangle \langle J_N || l_0 M_J(q) || J_N\rangle^* \Big)\Big] \\
&+ \frac{q^2}{2m_N^2} \sum_{J=2,4,\ldots}^{\infty} \Big( \langle J_N || \vec{l}_E \tilde{\Phi}'_J(q) || J_N\rangle \cdot \langle J_N || \vec{l}_E \tilde{\Phi}'_J(q) || J_N\rangle^* - |\langle J_N || \vec{l}_E \tilde{\Phi}'_J(q) || J_N\rangle|^2 \Big) \\
&+ \sum_{J=1,3,\ldots}^{\infty} \frac{1}{2}\Big( \langle J_N || \vec{l}_5 \Sigma'_J(q) || J_N\rangle \cdot \langle J_N || \vec{l}_5 \Sigma'_J(q) || J_N\rangle^* - |\langle J_N || \vec{l}_5 \Sigma'_J(q) || J_N\rangle|^2 \Big)\Bigg\}
\end{aligned} \tag{3.47}$$

Under the assumption that the dark matter/kinematics amplitude $l_i$ can be separated from the nuclear matrix elements it is then possible to see which response functions will contribute to the total scattering amplitude.

Table 3.6: Table of active dark matter and nuclear response functions within scalar dark matter constraints.

| Dark matter response function $R_O(\vec{v}_T^{\perp 2}, \vec{q}^2)$ | Nuclear response function $W_O(y)$ |
|---|---|
| $R_M(\vec{v}_T^{\perp 2}, \vec{q}^2) = c_1^2$ | $W_M(y) = \sum_{J=0,2,...}^{\infty} \langle j_N\|\|M_J(q)\|\|j_N\rangle \langle j_N\|\|M_J(q)\|\|j_N\rangle$ |
| $R_{\Phi''}(\vec{v}_T^{\perp 2}, \vec{q}^2) = \frac{1}{4}\vec{q}^2 c_3^2$ | $W_{\Phi''}(y) = \sum_{J=0,2,...}^{\infty} \langle j_N\|\|\Phi''_J(q)\|\|j_N\rangle \langle j_N\|\|\Phi''_J(q)\|\|j_N\rangle$ |
| $R_{\Phi'' M}(\vec{v}_T^{\perp 2}, \vec{q}^2) = c_3 c_1$ | $W_{\Phi'' M}(y) = \sum_{J=0,2,...}^{\infty} \langle j_N\|\|\Phi''_J(q)\|\|j_N\rangle \langle j_N\|\|M_J(q)\|\|j_N\rangle$ |
| $R_{\Sigma''}(\vec{v}_T^{\perp 2}, \vec{q}^2) = \frac{1}{4}\vec{q}^2 c_{10}^2$ | $W_{\Sigma''}(y) = \sum_{J=1,3,...}^{\infty} \langle j_N\|\|\Sigma''_J(q)\|\|j_N\rangle \langle j_N\|\|\Sigma''_J(q)\|\|j_N\rangle$ |
| $R_{\Sigma'}(\vec{v}_T^{\perp 2}, \vec{q}^2) = \frac{1}{8}\left[\vec{q}^2 \vec{v}_T^{\perp 2} c_3^2 + \vec{v}_T^{\perp 2} c_7^2\right]$ | $W_{\Sigma'}(y) = \sum_{J=1,3,...}^{\infty} \langle j_N\|\|\Sigma'_J(q)\|\|j_N\rangle \langle j_N\|\|\Sigma'_J(q)\|\|j_N\rangle$ |

With the response functions given in table 3.6 the scattering probability is now given by eq. (3.48).

$$\overline{|\mathcal{M}|^2}^{\text{elastic}}_{\text{nucleus}/Eff} = \frac{4\pi}{2J_i+1}\Bigg\{\Bigg[R_M(\vec{v}_T^{\perp 2}, \vec{q}^2)W_M(y) + R_{\Sigma''}(\vec{v}_T^{\perp 2}, \vec{q}^2)W_{\Sigma''}(y) + R_{\Sigma'}(\vec{v}_T^{\perp 2}, \vec{q}^2)W_{\Sigma'}(y)\Bigg] + \frac{\vec{q}^2}{m_N^2}\Bigg[R_{\Phi''}(\vec{v}_T^{\perp 2}, \vec{q}^2)W_{\Phi''}(y) + R_{\Phi'' M}(\vec{v}_T^{\perp 2}, \vec{q}^2)W_{\Phi'' M}(y)\Bigg]\Bigg\} \tag{3.48}$$

It is now important to note that $\mathcal{O}_1$ and $\mathcal{O}_3$ interfere with each other. This can be seen from the dark matter response $R_{\Phi'' M}$ in table 3.6. In order illustrate this we consider an interaction independent of the dark matter spin, but dependent on the nuclear spin and scattering kinematics [26].

$$\mathcal{L}_{int} = P^\mu \bar{\chi}\chi \bar{N} i\sigma_{\mu\nu} q^\nu N \tag{3.49}$$

Where $P^\mu = p^\mu + p'^\mu$ and $q^\mu = p'^\mu - p^\mu = k'^\mu - k^\mu$. The non-relativistic limit of this interaction is then written

$$\mathcal{L}_{int}^{Non-rel} = -(4m_\chi^2)q^2 + 16 m_N m_\chi^2 i v^\perp \cdot (q \times \vec{S}_N). \tag{3.50}$$

This in turn corresponds to the linear combination of operators

$$\mathcal{L}_{int}^{Eff} = -4m_\chi^2 q^2 \mathcal{O}_1 - 16 m_n m_\chi^2 \mathcal{O}_3. \tag{3.51}$$

Such an interaction would yield the interference mentioned above, i.e the scattering probability would be

$$P \propto c_1^2\alpha + c_3^2\beta + c_1 c_3 \gamma \tag{3.52}$$

where $\alpha$, $\beta$ and $\gamma$ include the dark matter and nuclear response.

## 3.5 Cross sections and rates

The observable in a direct detection experiment is the recoil energy $E_R$, from the dark matter-nucleus scattering process. In turn, this means that the event rate $\frac{dR}{dE_R}$

is also an observable. This quantity has a direct relation to the scattering cross section, where the cross section is given by (3.53) [36, 35].

$$d\sigma = \frac{1}{v}\frac{m_\chi}{E_\chi^i}\overline{|\mathcal{M}|^2}\frac{m_\chi}{E_\chi^f}\frac{d^3p'}{(2\pi)^3}\frac{m_T}{E_T^f}\frac{d^3k'}{(2\pi)^3}(2\pi)^4\delta^{(4)}(p+k-p'-k') \tag{3.53}$$

Where $E_\chi^i$ and $E_\chi^f$ is the initial and final energy of the dark matter particle, and $E_T^f$ is the final energy for the target nuclei.

With this cross section being in the lab frame of reference, $v$ is just the initial dark matter velocity where the target nuclei is at rest. Here $p$ and $p'$ is the initial and final dark matter momentum, thus $k$ and $k'$ is the initial and final nucleus momenta. In this non-relativistic context $\mathcal{M}$ is the Galilean invariant amplitude for dark matter-nucleus scattering (see eq. (3.48)), where $m_\chi$ and $m_T$ is the mass of the dark matter particle, and the target nuclei [36].

Since the amplitude $\mathcal{M}$ depends on $\vec{v}$ and $\vec{q}$, the differential cross section can be written as a function depending on two variables. By defining the scattering angle with the direction of the nuclear recoil relative to the initial dark matter velocity $\hat{v}\cdot\hat{k}' = -\hat{v}\cdot\hat{q} = cos(\theta)$, these variables are taken to be $\vec{v}$ and $\vec{q}^{\,2}$. The latter is equivalent to the recoil energy, since $E_R = \vec{q}^{\,2}/2m_T$. Integrating eq. (3.53) then gives the following expression [36].

$$\frac{d\sigma(v,E_R)}{dE_R} = 2m_T\frac{d\sigma(v,\vec{q}^{\,2})}{d\vec{q}^{\,2}} = \frac{m_T}{2\pi v^2}\overline{|\mathcal{M}|^2} \tag{3.54}$$

The differential event rate per target nuclei is then calculated through averaging over the galactic dark matter distribution [36].

$$\begin{aligned}\frac{dR_D}{dE_R} = N_T\frac{dR_T}{dE_R} = N_T\int\frac{d\sigma(v,E_R)}{dE_R}v\,dn_\chi = N_T n_\chi\int_{v>v_{\min}}\frac{d\sigma(v,E_R)}{dE_R}v f_E(\vec{v})d^3v\\ \equiv N_T\left\langle v\frac{d\sigma(v,E_R)}{dE_R}\right\rangle_{v>v_{\min}}\end{aligned} \tag{3.55}$$

Here $N_T$ is the number of target nuclei, $\rho_\chi$ is the local dark matter density, $n_\chi = \rho_\chi/m_\chi$ and $f_E(\vec{v})$ is the velocity distribution for the dark matter particles in the laboratory frame [36].

In experiments the observed differential event rate might differ from the actual event rate corresponding to the background excess we want to measure. Thus a more general expression for the event rate can be written as in (3.56) [34].

$$\left.\frac{dR}{dE_R}\right|_{\text{observed}} = S(E)\frac{dR_D}{dE_R} \tag{3.56}$$

where $S$ is the modified spectral function which takes into account detector efficiency and instrumental resolution [34].

This consequently means that when we want to integrate over the differential event rate in order to get the total number of events, the integral will be more complex due to some of the correction factors energy dependence, i.e

$$N_{\text{total}} = \text{Exposure} \cdot \int\limits_{E_{\min}}^{E_{max}} dE_R S(E_R) \frac{dR_D}{dE_R} \tag{3.57}$$

where the exposure is a product of the effective detector mass and time of testing. Here, $E_{\min}$ and $E_{\max}$ is energy threshold of the detector. This means that $E_{\max} - E_{\min} =$ signal region.

# 4
# Method

This section describes the statistical method used and how it is implemented with respect to the problem in question. In addition, the Monte Carlo algorithm used in the simulation of dark matter-nucleus scattering events is reviewed here. The last subsection describes the choices made for the various different model parameters used in this thesis.

## 4.1 Likelihood ratio test

The likelihood ratio test is a way of comparing two hypotheses with the use of a certain test statistic $q$. These Hypotheses correspond to a specific theoretical prediction for discreetly measured data, for example the expected number of scattering events in a given energy interval. These intervals will from now on be called bins. By sampling the test statistic $q$ enough times under each hypothesis a distribution of $q$ values can be constructed. Based on this, it is possible to make a qualitative statement about how many measured events one needs in order to reject one hypothesis in favour of the other with a significance $Z$ [17].

### 4.1.1 General approach to likelihood ratio tests

If we consider an experiment where the measured output for an event is a single kinematic variable, then it is possible to represent this output as histograms by binning the data. The theoretical expectation value is then written as in eq. (4.1) [17],

$$E[n_i] = \mu s_i + b_i \tag{4.1}$$

where $\mu$ is a strength parameter for the signal process, i.e $\mu = 0$ corresponds to $b_i$ background only events in the ith bin. $n_i$ is the ith entry in the aforementioned histogram and $s_i$ is the expected signal in question. The number of signal and background events in the ith bin is then given by eq. (4.2) [17].

$$\begin{aligned} s_i &= \int_{\text{bin } i} f_s(x; \boldsymbol{\theta}_s) dx \\ b_i &= \int_{\text{bin } i} f_b(x; \boldsymbol{\theta}_b) dx \end{aligned} \tag{4.2}$$

Here $f_s(x; \boldsymbol{\theta}_s)$ and $f_b(x; \boldsymbol{\theta}_b)$ are probability density functions depending on the variable $x$. $\boldsymbol{\theta}_{s,b}$ are parameters that affect the shape of the pdfs, these so called nuisance parameters are not considered as known beforehand and thus they will have to be fitted to the signal data later on [17]. In our case, however, there are none of these nuisance parameters. In our analysis, $f_s$ ($f_b$) is the unit normalised rate of signal (background) events in the ith energy bin, and $x$ is the nuclear recoil energy.

A control sample can be thought of in the same way as in eq. (4.1), i.e $E[m_i] = u \cdot \boldsymbol{\theta}$, where $m_i$ is the ith entry in the histogram corresponding to the control sample. Here $\boldsymbol{\theta}$ contains all nuisance parameters. This data could then for example consist of mainly background events. The likelihood function is then constructed from the product of Poisson likelihoods, one for each of the $N$ bins [17],

$$\mathcal{L}(\mu, \boldsymbol{\theta}) = \prod_{j=1}^{N} \frac{(\mu s_j + b_j)^{n_j}}{n_j!} e^{-(\mu s_j + b_j)} \prod_{k=1}^{M} \frac{u_k^{m_k}}{m_k!} e^{-u_k} \tag{4.3}$$

The likelihood ratio then becomes

$$\lambda(\mu) = \frac{\mathcal{L}(\mu, \hat{\hat{\boldsymbol{\theta}}})}{\mathcal{L}(\hat{\mu}, \hat{\boldsymbol{\theta}})} \tag{4.4}$$

where $\hat{\hat{\boldsymbol{\theta}}}$ is the values of $\boldsymbol{\theta}$ that maximises the likelihood function $\mathcal{L}$ for a specified value of $\mu$, i.e the numerator is the conditional maximum-likelihood. Meanwhile $\hat{\boldsymbol{\theta}}$ is the values of $\boldsymbol{\theta}$ that maximises the unconditional $\mathcal{L}$, that is the denominator. The test statistic $q$ can then easily be formed as in eq. (4.5) [17],

$$q = -2ln\lambda(\mu) \tag{4.5}$$

The reason for the $-2$ and the logarithm is that if we have nested hypotheses, and model parameters in the interior of the parameter space, $q$ will asymptotically approach a $\chi^2$-distribution [47].

### 4.1.2 Likelihood ratio test for discrete symmetries in scalar dark matter direct detection experiments

By recalling table 3.5 we have three distinct cases of transformation properties under $P$ and $CP$ in scalar dark matter-nucleus interactions. This allows us to form three hypotheses based on these properties.

Table 4.1: Table of the hypotheses studied in this thesis.

| | $H_0$ | $H_{A1}$ | $H_{A2}$ |
|---|---|---|---|
| Effective operators | $c_1\mathcal{O}_1 + c_3\mathcal{O}_3$ | $c_7\mathcal{O}_7$ | $c_{10}\mathcal{O}_{10}$ |
| $P$ | $+1$ | $-1$ | $-1$ |
| $CP$ | $+1$ | $+1$ | $-1$ |

$H_0$ corresponds to $P$ and $CP$ preserving dark matter-nucleus interactions. Our alternative hypotheses are $H_A = H_{A1}$, corresponding to parity violating, but $CP$ preserving interactions, and $H_A = H_{A2}$, corresponds to parity and $CP$ violating interactions.

Note that the hypotheses in question are not nested (i.e $H_A$ can not be mapped into $H_0$) and thus Wilks' theorem does not apply here. The expectation value for each bin is simply given by eq. (3.57), but integrated over each energy bin instead of the total range.

$$s_i(\boldsymbol{\theta}) = \text{Exposure} \cdot \int_{E_i}^{E_{i+1}} dE_R S(E_R) \frac{dR_D}{dE_R}. \tag{4.6}$$

For a given exposure, couplings constant and dark matter particle mass, each hypothesis will then correspond to a unique histogram of expected number of events, and can statistically be compared with the other hypotheses. For a given hypothesis, the measured data can then be simulated by sampling values from a Poisson distribution with expectation equal to that of the hypothesis for each of the $N$ energy bins.

$$d = [n_1, n_2, ..., n_N] \tag{4.7}$$

The likelihood function can then be written as in eq. (4.8), without considering a control sample,

$$\mathcal{L}(d, \boldsymbol{\theta}) = \prod_{i=1}^{N} \frac{e^{-S_i(\boldsymbol{\theta})}}{n_i!} \Big(S_i(\boldsymbol{\theta})\Big)^{n_i}. \tag{4.8}$$

Here, we assume $b_i = 0$.

The model parameters here are all parameters in the model that are not known a priori, that is $\boldsymbol{\theta} = (c_1, c_3, c_7, c_{10}, m_\chi)$. However, because of computational constraints, the dark matter mass $m_\chi$ will not be considered as a model parameter any further (see section 4.3). The shorthand notation $\theta_{0,A1,A2} = (c_1, c_3; c_7; c_{10})$ will also often be used instead of explicitly writing down the coupling coefficients.

It is now possible to write down the likelihood ratio by maximising the likelihood functions with respect to the respective model parameters.

$$\lambda = \frac{\mathcal{L}(d, \hat{\theta}_0)}{\mathcal{L}(d, \hat{\theta}_A)} \tag{4.9}$$

This in turn gives the expression for the test statistic $q$

$$q = -2ln\lambda = -2ln\left(\frac{\mathcal{L}(d, \hat{\theta}_0)}{\mathcal{L}(d, \hat{\theta}_A)}\right) \tag{4.10}$$

We can now see in eq. (4.10) that if $d$ is generated under assumption of the null hypothesis then $\mathcal{L}(d, \hat{\theta}_0) > \mathcal{L}(d, \hat{\theta}_A)$ should happen to most of the data samples, but if $d$ is generated under one of the alternative hypotheses instead, then $\mathcal{L}(d, \hat{\theta}_0) < \mathcal{L}(d, \hat{\theta}_A)$. Thus we expect that a distribution of $q$-values under the null hypothesis would be predominately negative and a distribution of $q$-values under one of the alternative hypotheses would predominately be positive.

By sampling $q$ enough times via Monte Carlo simulations we can then integrate the tail of the distribution under $H_0$ from the median of the distribution under $H_A$ ($q^A_{med}$) in order to get the $P$-value, i.e the probability that one realisation of the data under $H_0$ yields as an extreme or more extreme outcome in eq. (4.10) than when the data is generated under $H_A$.

$$P = \int_{q^A_{med}}^{\infty} f(q, \theta_0) dq \tag{4.11}$$

Here $f(q, \theta_0)$ is the distribution of $q$ under $H_0$. The significance for rejecting $H_0$ in favour of $H_A$ can be calculated from the inverse of the cumulative distribution of a standard Gaussian [17],

$$Z = \Phi^{-1}(1 - P). \tag{4.12}$$

When integrating $f(q, \theta_0)$, each $q$-value is assumed to be Gaussian and then weighed together in order to create a smooth distribution. The command **SmoothKernelDistribtution** in Mathematica is used for this. More about this method can be read in appendix D in [25].

## 4.2 Monte Carlo algorithm

In this section a flow chart for the Monte Carlo algorithm used is presented. The ith likelihood function $\mathcal{L}_i(d, \theta_{(0,A)})$ simply denotes

$$\mathcal{L}_i(d, \theta_{(0,A)}) = \frac{e^{-S_i(\boldsymbol{\theta})}}{n_i!}\Big(S_i(\boldsymbol{\theta})\Big)^{n_i} \tag{4.13}$$

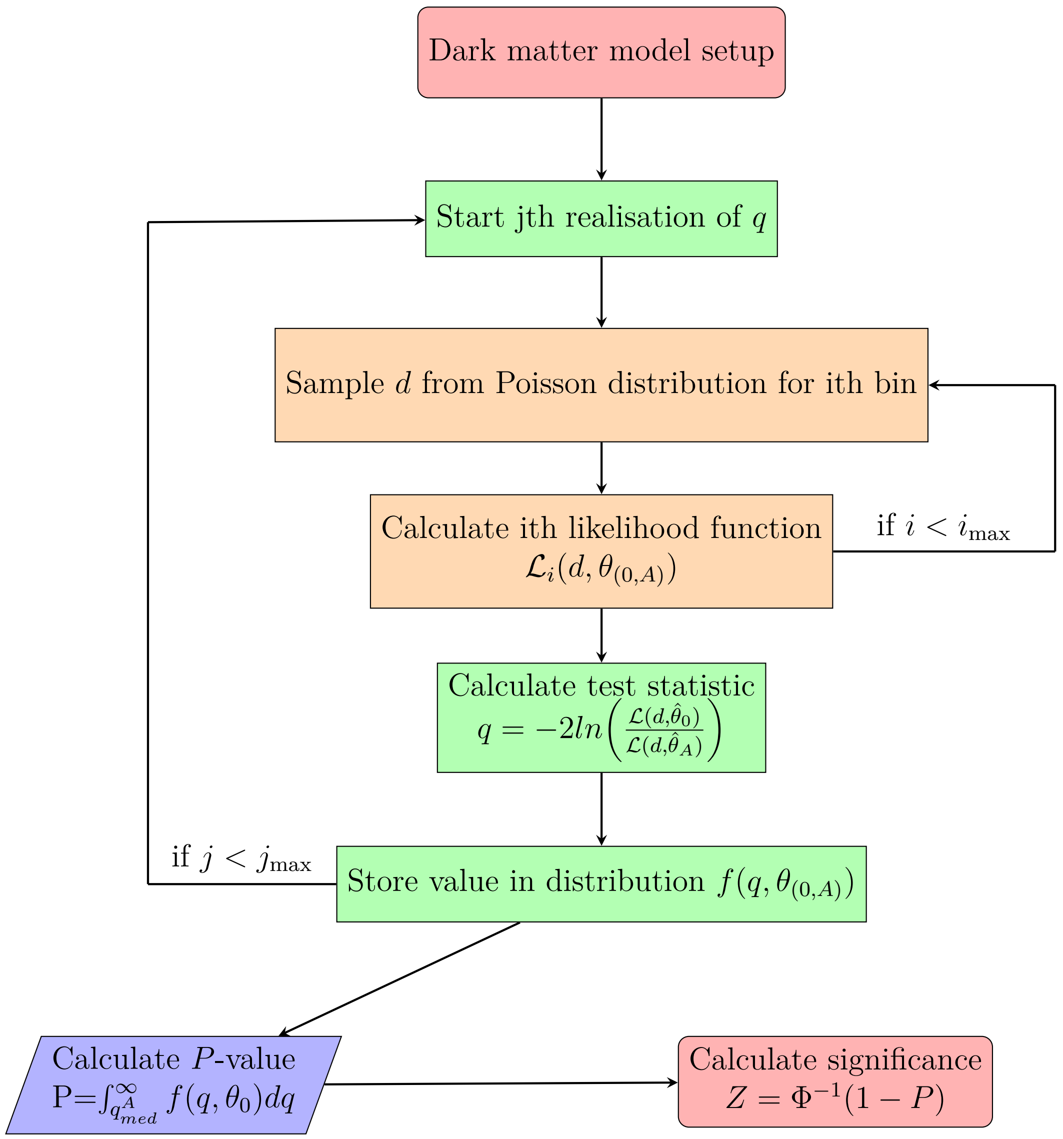


Figure 4.1: Illustrative flow chart for the Monte Carlo algorithm implemented.

For the maximisation process a random search algorithm is used with 40 starting guesses, which from these points uses another local optimisation method. This corresponds to the **RandomSearch** command in Mathematica.

## 4.3 Mock experiment setup

This subsection describes the choices made when setting up the dark matter model for the simulation of dark matter-nucleus scattering events. The assumptions and approximations made for the mock experiment are also described here, such as various different values for certain parameters.

As mentioned in section 4.1 the mass will not for computational reasons be considered as a model parameter. This means that the mass is taken as known beforehand and consequently is not maximised over in the likelihood function. This is in reality not the case, but adding the mass as a model parameter would mean that a 3-dimensional optimisation problem would be solved for each iteration of $q$. This would significantly increase the time it takes to run the code and would not be possible to do within the time frame allocated for this thesis project.

The choice of mass is however made to correspond with the current best set exclusion limit for a direct detection experiment. That is a spin independent dark matter-nucleon cross section for a 30 GeV dark matter particle at $\sigma_{SI} = 4.1 \cdot 10^{-47}$ cm$^2$ set by the Xenon1t experiment [3]. The coupling coefficient for $\mathcal{O}_1$ is then given by the relation in eq. (4.14) [36].

$$\sigma_N = \frac{1}{\pi}\left(\frac{c_{1,exc}}{m_v^2}\right)^2 \mu_{NT}^2, \quad \mu_{NT} = \frac{m_N m_T}{m_N + m_T} \tag{4.14}$$

Where the coupling coefficient is normalised with the Higgs expectation value $m_v = 246.2$ GeV. By assuming the same coupling to protons and neutrons, the exclusion limit is guaranteed to be preserved.

In order to construct a model for the null hypothesis, $c_3$ needs to be determined as well. As can be seen in eq. (3.52) the amplitude and consequently the rate for the Null hypothesis depends on three terms.

$$\frac{dR_D}{dE_R} \propto c_1^2\alpha + c_3^2\beta + c_1 c_3 \gamma \tag{4.15}$$

From this relation, three different null hypotheses will be formulated. One with a dominating $\mathcal{O}_1$ response and one with a dominating $\mathcal{O}_3$ response, but in addition a democratic response is formulated as well. In this null hypothesis, $c_3$ is chosen so that the $c_3^2$ term of the rate contribute equally to total rate, and thus the total number of events, as the $c_1^2$ term. When $\mathcal{O}_1$ is dominating, the $c_3^2$ term is taken to contribute with a factor $10^{-3}$ less than the $c_1^2$ term. In the same way when $\mathcal{O}_3$ is dominating, $c_3^2$ is chosen to contribute with a factor $10^3$ more than the $c_1^2$ term. When solving for a coupling coefficient, two solutions will always be available, thus the positive one will always be chosen. This only matters however in the interference term in $H_0$. These three null hypothesis are defined in table 4.2.

In order to compare the alternative hypotheses with the null hypotheses, the coupling coefficients $c_7$ and $c_{10}$ are chosen so that they produce the same total number of expected events over the whole energy range as $H_0$.

In figure 4.2 the differential event rate is shown for each of the operators separately, i.e the linear combination of $c_1\mathcal{O}_1 + c_3\mathcal{O}_3$ is not plotted. For the tyranny case

Table 4.2: Table of defined null hypothesis.

| Type: | Defined relation: |
|---|---|
| Democratic | $\frac{dR_D}{dE_R}(c_1,0) = \frac{dR_D}{dE_R}(0,c_3)$ |
| Tyranny $\mathcal{O}_1$ | $\frac{dR_D}{dE_R}(c_1,0) = 10^{-3} \cdot \frac{dR_D}{dE_R}(0,c_3)$ |
| Tyranny $\mathcal{O}_3$ | $\frac{dR_D}{dE_R}(c_1,0) = 10^{3} \cdot \frac{dR_D}{dE_R}(0,c_3)$ |

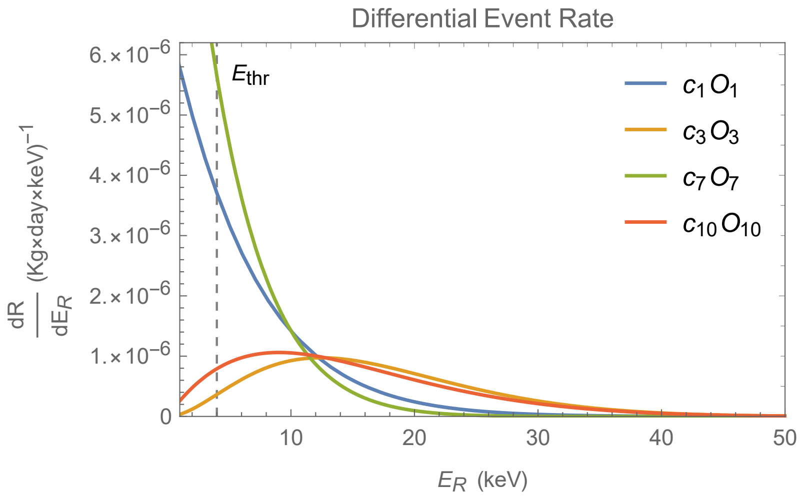


Figure 4.2: The recoil spectrum corresponding to each operator when all coupling coefficients are solved to yield the same number of total events in the complete energy range as $\mathcal{O}_1$.

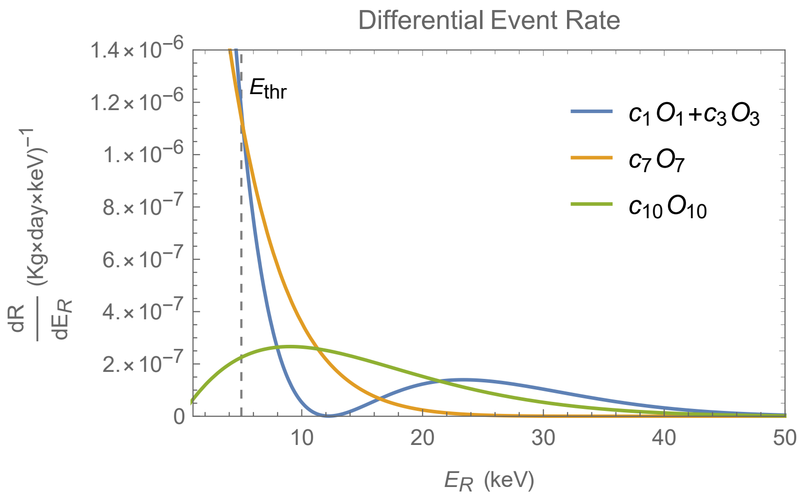


Figure 4.3: The recoil spectrum for the democratic $H_0$ and the two alternative hypothesis fitted such that they produce the same number of total events over the whole energy range as $H_0$.

of the null hypothesis, this plot yields the same shape as the respective tyrannical case. In figure 4.3 the democratic case is shown instead.

The direct detection experiment will be modelled in a similar manner as in [32]. That is, we assume an infinite energy resolution past a constant efficiency of $\varepsilon = 0.7$. The expected number of events in each bin is then given by

$$S_i(\boldsymbol{\theta}) = \text{Exposure} \cdot \varepsilon \cdot \int_{E_\text{i}}^{E_{i+1}} dE_R \frac{dR_D}{dE_R} \tag{4.16}$$

The energy range for integration is chosen to be from 5 keV to 50 keV, which is the typical recoil energy range. We will also impose a cutoff for the analysis at a couple of events in return for the approximation that there is no background noise, thus the likelihood function is given by

$$\mathcal{L}(d, \boldsymbol{\theta}) = \prod_{i=1}^{N} \frac{e^{-(S_i(\boldsymbol{\theta}))}}{n_i!} \Big( S_i(\boldsymbol{\theta}) \Big)^{n_i} \tag{4.17}$$

The target nuclei will be set to the commonly used xenon-131. Xenon is among other experiments used in the XENON1T experiment [3], and will also be used in the upcoming LUX-ZEPLIN experiment [14], thus it makes for a natural choice.

The standard value for the dark matter density is used $\rho_\chi = 0.3$ GeV/cm$^3$ and the cutoff for the Boltzmann distribution, i.e the escape velocity is set to $v_{esc} =$ 550 km/s. The velocity for the earth is $v_e = 232$ km/s and $v_0$ in the Boltzmann distribution

$$f_v(\vec{v}) = \frac{1}{\pi^3 v_o^3} e^{-v^2/v_0^2} \tag{4.18}$$

is taken as $v_0 = 220$ km/s [32, 36].

# 5

# Results

In this section the results are presented. All histogram-plots are distributions of the test statistic $q$ given in (4.10). The distributions in red are the distributions of q-values generated assuming $H_0$ and the the distributions in blue are generated assuming $H_A$.

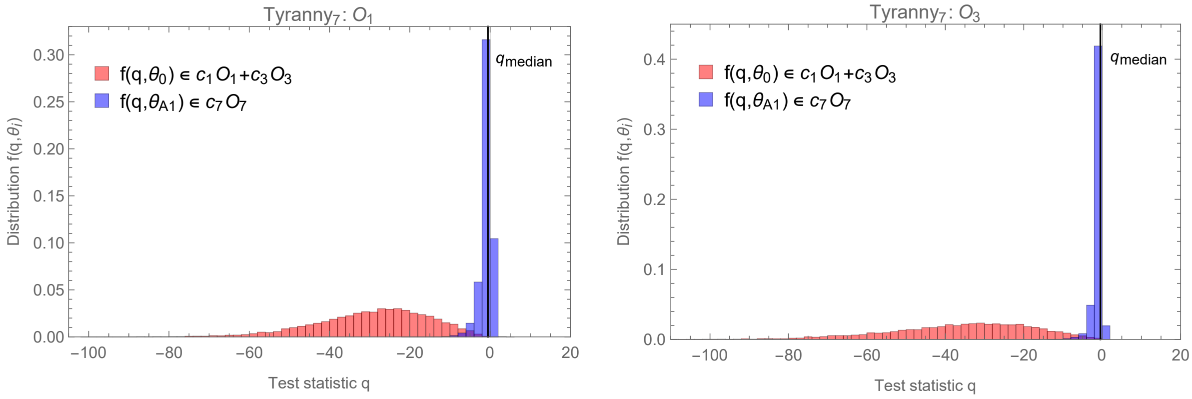


(a) Tyrannical $\mathcal{O}_1$ where $Z \approx 3.1\sigma$.

(b) Tyrannical $\mathcal{O}_3$ where $Z \approx 3.1\sigma$.

Figure 5.1: Distributions for both tyrannical cases when considering the alternative hypothesis $\mathcal{O}_7$.

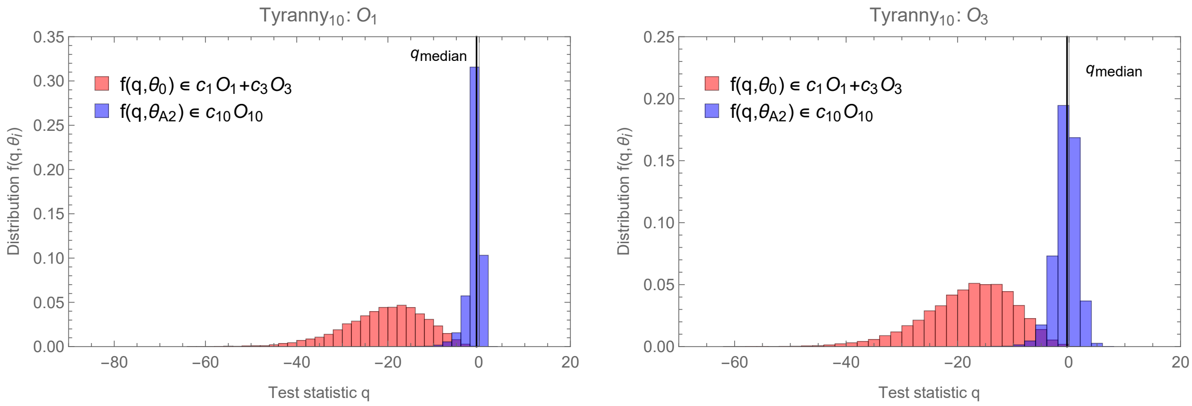


(a) Tyrannical $\mathcal{O}_1$ where $Z \approx 3.3\sigma$.

(b) Tyrannical $\mathcal{O}_3$ where $Z \approx 3.0\sigma$.

Figure 5.2: Distributions for both tyrannical cases when considering the alternative hypothesis $\mathcal{O}_{10}$.

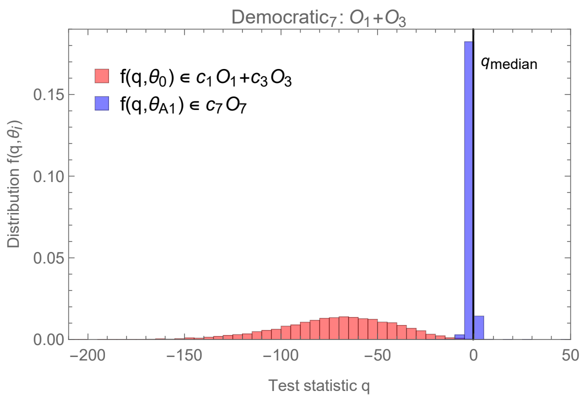


(a) Democratic case when considering $H_A \in \mathcal{O}_7$. Here $Z \approx 3.3\sigma$.

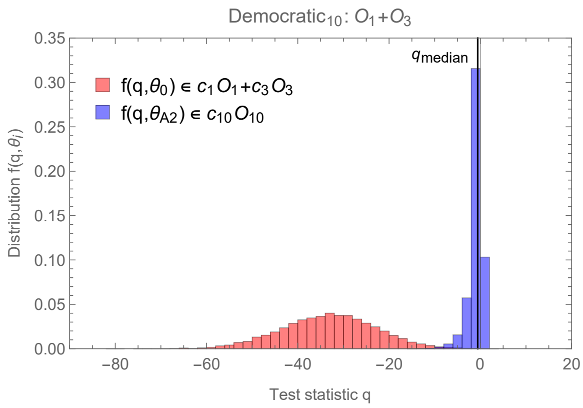


(b) Democratic case when considering $H_A \in \mathcal{O}_{10}$. Here $Z \approx 3.4\sigma$.

Figure 5.3: Distributions for both democratic cases.

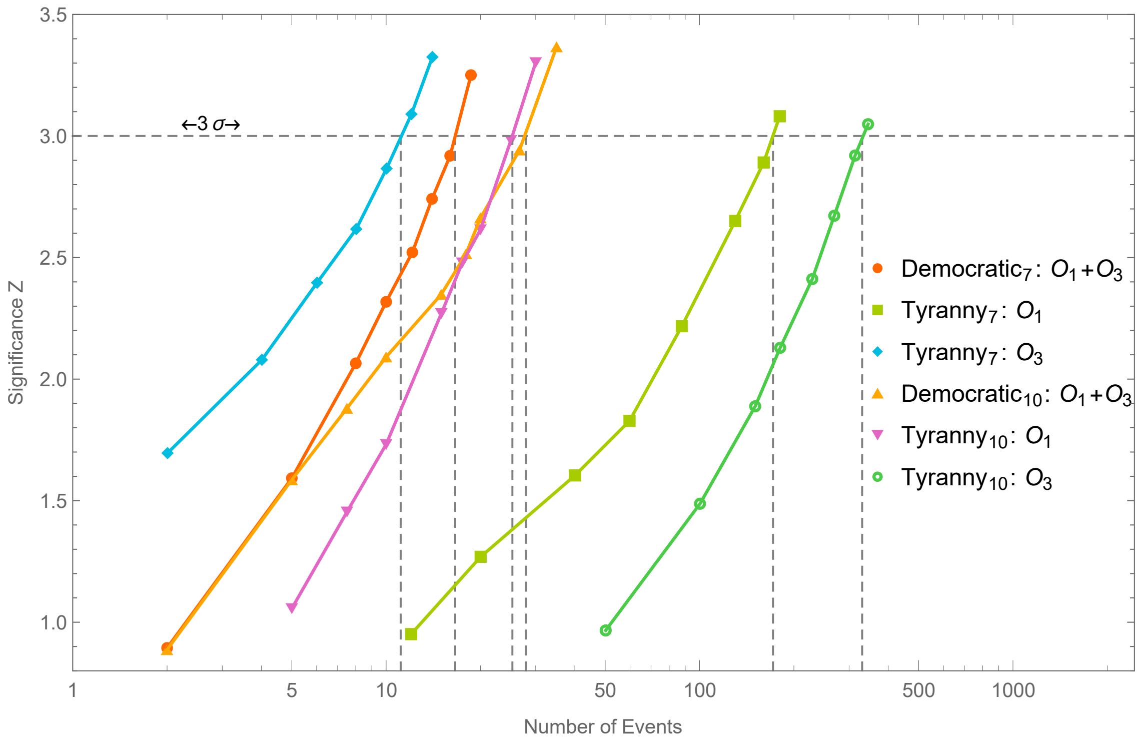


Figure 5.4: Plot of how many scattering events are required in order to reject $H_0$ in favour of $H_A$ with a significance $Z$. The three different cases of $H_0$ are shown here when each case is compared to either $H_{A1} \in \mathcal{O}_7$ or $H_{A2} \in \mathcal{O}_{10}$. Which alternative hypothesis is considered is denoted by the subindex 7 or 10. The three different cases of $H_0$ are denoted Tyranny: $\mathcal{O}_1$, Tyranny: $\mathcal{O}_3$ and Democratic: $\mathcal{O}_1 + \mathcal{O}_3$. Each dot corresponds two distributions of q-values under a specific $H_A$ and $H_0$, which are used in order to calculate the significance .

# 6
# Discussion

In figure 5.4 we can see that it is possible with a $3\sigma$ significance to reject the null hypothesis in favour of the alternative hypothesis when the number of signal events is $\mathcal{O}(10)$. We can also see that which operator is dominating makes a big difference in the number of events required. This is in accordance with what is expected from figure 4.2. The similarities in the spectrum of $\mathcal{O}_1$ and $\mathcal{O}_7$ does indeed show that more events are required in order to discriminate between the two hypotheses, when $\mathcal{O}_1$ is dominating. However, when $\mathcal{O}_3$ is dominating, this amount is greatly reduced to only requiring about 10 events.

The same is true in the case of $\mathcal{O}_{10}$, but then the tyrannical $\mathcal{O}_3$ case requires a lot more events instead. It can also be seen from figure 5.4 that the democratic case seams to require about the same number of events, which is in accordance of what is expected from figure 4.3.

These results show that in direct detection experiments it is indeed possible to get information concerning the properties of scalar dark matter-nucleus interactions under the discrete transformations $P$ and $CP$. It should however be noted that the model that constitutes the null hypothesis, i.e $c_1\mathcal{O}_1 + c_3\mathcal{O}_3$ is a very flexible model which can be seen from the fact the the distributions under alternative hypotheses peak on the left side of the origin. This means that for the given exposure the null hypothesis is a better fit for the data generated under the alternative hypothesis, than the alternative hypothesis in question. It is still possible to reject $H_0$ in favour of $H_A$, since if the data is generated under $H_0$ the distribution is far more on the negative side of the origin, not fluctuating around it.

The flexibility of the model does mean a "worse" case scenario can be constructed. This would mean, constructing a null hypothesis where the model choice for $c_1$ and $c_3$ have been fitted to one realisation of data generated under $H_A$. This would greatly increase the exposure and in turn the number of events by orders of magnitude needed in order to discriminate between the two hypotheses, and would not be within the reach of next generation direct detection experiments, as would be the case of the other models constructed. This does mean that not all possible P and CP-conserving scalar dark matter nucleus interactions are rejected, but this thesis shows that it is indeed possible to discriminate between P and CP-transformation properties within the context of the effective theory describing the interactions in the direct detection experiments. Depending on the model choice for $H_0$ it can also be within the range of next generation direct detection experiments.

As already mentioned in the thesis, the dark matter mass is not considered a model parameter. The statistical analysis could be improved by including this as a parameter to be maximised with respect to.

In this thesis, some approximations regarding the event rate was also made. The analysis could be improved by considering background event rate and a finite energy resolution and an energy dependent experimental efficiency.

# 7
# Conclusion

From figure 5.4 it can be seen that it is indeed possible to discriminate between different cases of $P$ and $CP$ transformations in scalar dark matter-nucleus interactions. When the alternative hypothesis is $\mathcal{O}_7$, for example we can see that for the tyrannical $\mathcal{O}_3$ case it would only require about 11 events in order to reject invariance under $P$ and $CP$ in favour of $P$ odd and $CP$ even. When $\mathcal{O}_1$ is dominating instead, this would require about 170 events and for the democratic case it would be approximately 17 events. This being with a $3\sigma$ significance.

When considering the second alternative hypothesis, i.e odd under both $P$ and $CP$, which corresponds to $\mathcal{O}_{10}$, the tyrannical $\mathcal{O}_3$ case would require 330 events. This is by far the most difficult case to discriminate between the two hypotheses, that being among the cases considered in this thesis. When $\mathcal{O}_1$ is dominating instead, this only requires about 25 events and for the democratic case this would be 28 events. This also being with a $3\sigma$ significance.

This statistical analysis could be improved by including the dark matter mass as a model parameter. Further investigations into this subject area might also want to consider modelling the energy dependency for the experimental efficiency and a finite energy resolution, thus taking into account some of the uncertainties not considered in this thesis.

# A

# Anapole Dark Matter

The Lagrangian for a Majorana fermion with spin-$\frac{1}{2}$ and anapole moment that interacts via photons can in Lorentz invariant form be written as in eq. (A.1) [37].

$$\hat{\mathcal{L}}_I = \frac{g}{2\Lambda^2}\bar{\chi}\gamma^\mu\gamma^5\chi\partial^\nu\hat{F}_{\mu\nu} \tag{A.1}$$

This can be rewritten in terms of the field strength tensor for the electromagnetic field.

$$\hat{\mathcal{L}}_I = \frac{g}{2\Lambda^2}\bar{\chi}\gamma^\mu\gamma^5\chi\partial^\nu\Big(\partial_\nu A_\mu - \partial_\mu A_\nu\Big) \tag{A.2}$$

With the use of partial integration it is possible to express the effective Lagrangian in terms of the current tensor.

$$\hat{\mathcal{L}}_I = \frac{g}{2\Lambda^2}\Big(g^{\mu\lambda}\partial^\nu\partial_\nu - \partial^\mu\partial^\lambda\Big)\bar{\chi}\gamma_\lambda\gamma^5\chi\hat{A}_\mu = -\hat{j}^\mu(\boldsymbol{x})\hat{A}_\mu(\boldsymbol{x}) \tag{A.3}$$

According to Fermi's golden rule for two-body scattering events the cross section is written as in eq. (A.4).

$$d\sigma_T = \frac{2\pi}{v}\delta(E_{P'} + \varepsilon_{k'} - E_P - \varepsilon_k)\overline{|T_{fi}|^2}\frac{d\boldsymbol{k'}}{(2\pi)^3} \tag{A.4}$$

Where $k$, $k'$, $P$ and $P'$ denotes the momentum before and after the scattering event for the DM-particle and the nucleus respectively. The leading order transition amplitude is given by the following expression.

$$\begin{aligned} S_{fi} &= -i\int d^4x \,\langle k', s', \lambda'|\hat{\mathcal{L}}_I(\boldsymbol{x})|k, s, \lambda\rangle \equiv i(2\pi)\delta(E_{P'} + \varepsilon_{k'} - E_P - \varepsilon_k)T_{fi} \\ &= -i\int d^4x \,\langle k', s'|\hat{j}^\mu(\boldsymbol{x})|k, s\rangle \,\langle\lambda'|\hat{A}_\mu(\boldsymbol{x})|\lambda\rangle \end{aligned} \tag{A.5}$$

Where $s$, $s'$, $\lambda$ and $\lambda'$ denotes the spin polarisations for the dark matter particle and the nucleus before and after interaction.

In the Schrödinger picture, the current tensor can be written as the translation of the current tensor at the origin, i.e

$$\hat{j}^\mu(\boldsymbol{x}) = \hat{j}^\mu(0)e^{-iqx} \tag{A.6}$$

Thus the matrix element can be written as a Fourier transform.

$$\begin{aligned} S_{fi} &= -i\,\langle k', s'|\hat{j}^\mu(0)|k, s\rangle \int d^4x e^{-iqx}\,\langle\lambda'|\hat{A}_\mu(\boldsymbol{x})|\lambda\rangle \\ &= -i\,\langle k', s'|\hat{j}^\mu(0)|k, s\rangle\,\langle\lambda'|\hat{A}_\mu(q)|\lambda\rangle \end{aligned} \tag{A.7}$$

## A.1 Calculation of DM matrix element

In order to calculate the matrix element for the current tensor, it is first expanded in terms of its derivatives.

$$\begin{aligned}\hat{j}^\mu(\boldsymbol{x}) = -\frac{g}{2\Lambda^2}\Bigg[g^{\mu\lambda}\Big(\partial^\nu\partial_\nu\bar{\chi}\gamma_\lambda\gamma_5\chi + \partial_\nu\bar{\chi}\gamma_\lambda\gamma_5\partial^\nu\chi + \partial^\nu\bar{\chi}\gamma_\lambda\gamma_5\partial_\nu\chi + \bar{\chi}\gamma_\lambda\gamma_5\partial^\nu\partial_\nu\chi\Big) \\ -\Big(\partial^\mu\partial^\lambda\bar{\chi}\gamma_\lambda\gamma_5\chi + \partial^\lambda\bar{\chi}\gamma_\lambda\gamma_5\partial^\mu\chi + \partial^\mu\bar{\chi}\gamma_\lambda\gamma_5\partial^\lambda\chi + \bar{\chi}\gamma_\lambda\gamma_5\partial^\mu\partial^\lambda\chi\Big)\Bigg]\end{aligned} \tag{A.8}$$

Majorana fermions are defined by $\chi = \chi^c$, i.e they are invariant under charge conjugation. Expanding $\chi$ in terms of creation and annihilation operators consequently gives $a_s(p) = b_s(p)$ and $a_s^\dagger(p) = b_s^\dagger(p)$. The creation and annihilation operators will from now on be denoted by $C_{rp}$, with spin polarisation $r$ and momentum $p$. The expansion can then be written

$$\chi = \int \frac{d^3P}{(2\pi)^3}\frac{1}{\sqrt{E_P}}\sum_{rp}\Big[C_{rp}u_{rp}e^{-iqx} + C_{rp}^\dagger\bar{u}_{rp}e^{iqx}\Big] = \bar{\chi} \tag{A.9}$$

Inserting this into the equation for the matrix element we have

$$\begin{aligned}&\langle k', s'|\hat{j}^\mu(0)|k, s\rangle = \\ &= \langle 0|C_{s'k'}\Bigg\{-\frac{g}{2\Lambda^2}\Bigg[g^{\mu\lambda}\Big(\int\frac{d^3k'}{(2\pi)^3}\frac{1}{\sqrt{2\varepsilon_{k'}}}\sum_{s'k'}(-q^2C_{s'k'}^\dagger\bar{u}_{s'k'})\gamma_\lambda\gamma_5\int\frac{d^3k}{(2\pi)^3}\frac{1}{\sqrt{2\varepsilon_k}}\sum_{sk}(C_{sk}u_{sk}) \\ &+\int\frac{d^3k'}{(2\pi)^3}\frac{1}{\sqrt{2\varepsilon_{k'}}}\sum_{s'k'}(iq_\nu C_{s'k'}^\dagger\bar{u}_{s'k'})\gamma_\lambda\gamma_5\int\frac{d^3k}{(2\pi)^3}\frac{1}{\sqrt{2\varepsilon_k}}\sum_{sk}(-iq^\nu C_{sk}u_{sk}) \\ &+\int\frac{d^3k'}{(2\pi)^3}\frac{1}{\sqrt{2\varepsilon_{k'}}}\sum_{s'k'}(iq^\nu C_{s'k'}^\dagger\bar{u}_{s'k'})\gamma_\lambda\gamma_5\int\frac{d^3k}{(2\pi)^3}\frac{1}{\sqrt{2\varepsilon_k}}\sum_{sk}(-iq_\nu C_{sk}u_{sk}) \\ &+\int\frac{d^3k'}{(2\pi)^3}\frac{1}{\sqrt{2\varepsilon_{k'}}}\sum_{s'k'}(C_{s'k'}^\dagger\bar{u}_{s'k'})\gamma_\lambda\gamma_5\int\frac{d^3k}{(2\pi)^3}\frac{1}{\sqrt{2\varepsilon_k}}\sum_{sk}(-q^2C_{sk}u_{sk})\Big) \\ &-\Big(\int\frac{d^3k'}{(2\pi)^3}\frac{1}{\sqrt{2\varepsilon_{k'}}}\sum_{s'k'}(-q^\mu q^\lambda C_{s'k'}^\dagger\bar{u}_{s'k'})\gamma_\lambda\gamma_5\int\frac{d^3k}{(2\pi)^3}\frac{1}{\sqrt{2\varepsilon_k}}\sum_{sk}(C_{sk}u_{sk}) \\ &+\int\frac{d^3k'}{(2\pi)^3}\frac{1}{\sqrt{2\varepsilon_{k'}}}\sum_{s'k'}(iq^\lambda C_{s'k'}^\dagger\bar{u}_{s'k'})\gamma_\lambda\gamma_5\int\frac{d^3k}{(2\pi)^3}\frac{1}{\sqrt{2\varepsilon_k}}\sum_{sk}(-iq^\mu C_{sk}u_{sk}) \\ &+\int\frac{d^3k'}{(2\pi)^3}\frac{1}{\sqrt{2\varepsilon_{k'}}}\sum_{s'k'}(iq^\mu C_{s'k'}^\dagger\bar{u}_{s'k'})\gamma_\lambda\gamma_5\int\frac{d^3k}{(2\pi)^3}\frac{1}{\sqrt{2\varepsilon_k}}\sum_{sk}(-iq^\lambda C_{sk}u_{sk}) \\ &+\int\frac{d^3k'}{(2\pi)^3}\frac{1}{\sqrt{2\varepsilon_{k'}}}\sum_{s'k'}(C_{s'k'}^\dagger\bar{u}_{s'k'})\gamma_\lambda\gamma_5\int\frac{d^3k}{(2\pi)^3}\frac{1}{\sqrt{2\varepsilon_k}}\sum_{sk}(-q^\mu q^\lambda C_{sk}u_{sk})\Big)\Bigg]\Bigg\}C_{sk}^\dagger\,|0\rangle\end{aligned} \tag{A.10}$$

This in turn can be simplified.

$$\langle k', s'|\hat{j}^\mu(0)|k, s\rangle = \hat{j}^\mu_{ss'} = \frac{g}{\Lambda^2}q^2\Big(g^{\mu\lambda} - \frac{q^\mu q^\lambda}{q^2}\Big)\frac{1}{\sqrt{2\varepsilon_{k'}2\varepsilon_k}}\bar{u}_{s'k'}\gamma_\lambda\gamma_5u_{sk} \tag{A.11}$$

In the non-relativistic limit, the solution to the Dirac equation is given by eq. (3.5).

$$u_s(p) = \frac{1}{\sqrt{4m}} \begin{pmatrix} (2m - \vec{p}\cdot\vec{\sigma})\xi^s \\ (2m + \vec{p}\cdot\vec{\sigma})\xi^s \end{pmatrix} + \mathcal{O}(\vec{p}^2) \tag{A.12}$$

The bilinear in eq (A.11) using chiral bases are as follow

$$\begin{aligned} \bar{u}_{s'k'}\gamma_\lambda\gamma_5 u_{sk} &\approx \frac{1}{\sqrt{4m}} \left(\xi^\dagger_{s'}(2m + \vec{k}'\cdot\vec{\sigma}), \xi^\dagger_{s'}(2m - \vec{k}'\cdot\vec{\sigma})\right) \\ &\cdot \begin{pmatrix} 0 & \sigma^\mu \\ -\bar{\sigma}^\mu & 0 \end{pmatrix} \frac{1}{\sqrt{4m}} \begin{pmatrix} (2m - \vec{k}\cdot\vec{\sigma})\xi_s \\ (2m + \vec{k}\cdot\vec{\sigma})\xi_s \end{pmatrix} \end{aligned} \tag{A.13}$$

$$= \frac{1}{4m}\left[\xi^\dagger_{s'}(2m + \vec{k}'\cdot\vec{\sigma})\sigma^\mu(2m + \vec{k}\cdot\vec{\sigma})\xi_s - \xi^\dagger_{s'}(2m - \vec{k}'\cdot\vec{\sigma})\bar{\sigma}^\mu(2m - \vec{k}\cdot\vec{\sigma})\xi_s\right]$$

Since $\sigma^\mu = (\mathbb{1}, \vec{\sigma})$ and $\bar{\sigma}^\mu = (\mathbb{1}, -\vec{\sigma})$. By ignoring higher order terms, the bilinear is simplified to the following expression

$$\bar{u}_{s'k'}\gamma_\lambda\gamma_5 u_{sk} = \frac{1}{4m}\left[4m(\vec{k}' + \vec{k})\cdot\xi^\dagger_{s'}\vec{\sigma}\xi_s + 8m^2\xi^\dagger_{s'}\vec{\sigma}\xi_s\right] \tag{A.14}$$

By denoting $\boldsymbol{s} = \xi^\dagger_{s'}\vec{\sigma}\xi_s$ and writing the scalar and vector parts of the bilinear separately we have

$$\bar{u}_{s'k'}\gamma_\lambda\gamma_5 u_{sk} = 2m\left(\frac{(\vec{k}' + \vec{k})}{2m}\cdot\boldsymbol{s}, \boldsymbol{s}\right) \tag{A.15}$$

Since $\hat{j}^\mu_{ss'}$ can be written in components of the probability current and current density we have in the non-relativistic limit the following equation for the current tensor at the origin.

$$\hat{j}^\mu_{ss'}(0) = \left(\rho^\chi_{ss'}(0), j^\chi_{ss'}(0)\right) = q^2\frac{g}{\Lambda^2}\left(g^{\mu\lambda} - \frac{q^\mu q^\lambda}{q^2}\right)\left(\frac{(\vec{k}' + \vec{k})}{2m}\cdot\boldsymbol{s}, \boldsymbol{s}\right) \tag{A.16}$$

In elastic scattering $(\vec{k} + \vec{k}')(\vec{k} - \vec{k}') = 0$ and since $q = \vec{k} - \vec{k}'$ it is possible to write both the time-component and the spatial components of $\hat{j}^\mu_{ss'}$ in terms of the component of $\boldsymbol{s}$ that is transverse to $q = \vec{k} - \vec{k}'$, i.e $\boldsymbol{s_T} = \boldsymbol{s} - \frac{\boldsymbol{s}\cdot\boldsymbol{q}}{|\boldsymbol{q}^2|}q$.

$$\begin{aligned} \rho^\chi_{ss'}(0) &= -|\boldsymbol{q}^2|\frac{g}{\Lambda^2}\frac{(\vec{k} + \vec{k}')}{2m}\cdot\boldsymbol{s_T} \\ j^\chi_{ss'}(0) &= -|\boldsymbol{q}^2|\frac{g}{\Lambda^2}\boldsymbol{s_T} \end{aligned} \tag{A.17}$$

Where $q^2 = -|\boldsymbol{q}^2|$.

## A.2 Calculation of Nuclear Matrix Element

In Lorenz gauge $\partial_\mu \hat{A}^\mu(x) = 0$, Maxwell's equations can be written

$$\Box \hat{A}^\mu(x) = e\hat{j}^\mu(x) \tag{A.18}$$

With the use of Heisenberg's equation of motion

$$\hat{j}^\mu(x) = e^{i\hat{H}_N t}\hat{j}^\mu(x)e^{-i\hat{H}_N t} \tag{A.19}$$

and by taking the Fourier transform of eq. (A.18), the field strength tensor can be written as an expression of the current tensor.

$$-q^2\hat{A}^\mu(q) = e2\pi\delta(E_{P'} + \varepsilon_{k'} - E_P - \varepsilon_k)\hat{j}^\mu(q) \tag{A.20}$$

Thus the nuclear matrix element in eq. (A.7) can be written as

$$\langle\lambda'|\hat{A}^\mu(q)|\lambda\rangle = -\frac{e}{q^2}2\pi\delta(E_{P'} + \varepsilon_{k'} - E_P - \varepsilon_k)\,\langle\lambda'|\hat{j}^\mu(q)|\lambda\rangle \tag{A.21}$$

The transition amplitude in eq. (A.5) can now be written as an expression of the current tensors

$$\begin{gathered}-i\hat{j}^\mu_{ss'}(0)\hat{j}^{\lambda\lambda'}_\mu(q)\cdot 2\pi\delta(E_{P'} + \varepsilon_{k'} - E_P - \varepsilon_k)\frac{e}{|\boldsymbol{q}^2|} = i2\pi\delta(E_{P'} + \varepsilon_{k'} - E_P - \varepsilon_k)T_{fi} \\ T_{fi} = -\frac{e}{|\boldsymbol{q}^2|}\hat{j}^\mu_{ss'}(0)\hat{j}^{\lambda\lambda'}_\mu(q)\end{gathered} \tag{A.22}$$

In terms of time and spatial components, the transition amplitude then becomes

$$T_{fi} = -\frac{e}{|\boldsymbol{q}^2|}\Big(\hat{j}^0_{ss'}(0)\hat{j}^{\lambda\lambda'}_0(q) - \hat{j}^\nu_{ss'}(0)\hat{j}^{\lambda\lambda'}_\nu(q)\Big) \tag{A.23}$$

Inserting eq. (A.17) into (A.23) we have

$$T_{fi} = \frac{eg}{\Lambda^2}\boldsymbol{s_T}\cdot\left(\frac{\vec{k}' + \vec{k}}{2m}\rho_{\lambda\lambda'}(q) - J_{\lambda\lambda'}(q)\right) \tag{A.24}$$

## A.3 Lab frame of reference

The nuclear charge and current density matrix elements are rewritten using the frame of reference defined in de Forest and Walecka [18]. To do this $J^\mu(q)$ is decomposed in the frame of references where the target nucleus is at rest and the $z$-axis is defined along the direction of momentum transfer, denoted by $\boldsymbol{q}_{lab}$. The de Forest and Walecka frame can be described in terms of the orthogonal four-vectors $P^\mu = (m_T, \vec{0})$, $q^\mu = \left(q^\mu - \frac{P\cdot q}{m_T}P^\mu\right)$ and $e^\mu_{\pm 1}$, where $e^\mu_{\pm 1}$ are spherical basis vectors

$\boldsymbol{e}_{\pm 1} = (\hat{\boldsymbol{x}} \pm \hat{\boldsymbol{y}})/\sqrt{2}$. By imposing conservation $J^\mu q_\mu = 0$, the decomposition of the current tensor in this frame of reference is written

$$J^\mu = \sum_{\alpha=1}^{3} J^\alpha e^\mu_\alpha \tag{A.25}$$

Where $\alpha = 1$ corresponds to the non-spatial part. One solution will in terms of a linear combination of $P^\mu$ and $q^\mu$ yield

$$aP^\mu + b\Big(q^\mu - \frac{P\cdot q}{m_T}P^\mu\Big) = \Big(P^\mu - \frac{P\cdot q}{q^2}q^\mu\Big) \tag{A.26}$$

Thus we have

$$J^\mu = J_1\Big(P^\mu - \frac{P\cdot q}{q^2}q^\mu\Big) + J_2 e^\mu_{+1} + J_3 e^\mu_{-1} \tag{A.27}$$

In the de Forest and Walecka frame $J^0$ is given by

$$J^0 = \frac{J\cdot P}{m_T}\bigg|_{FW} \equiv \rho^{lab} = J_1\frac{P^2}{m_T} = J_1 m_T \to J_1 = \frac{\rho^{lab}}{m_T} \tag{A.28}$$

This gives the expression

$$J^\mu = \frac{\rho^{lab}}{m_T}\Big(P^\mu - \frac{P\cdot q}{q^2}q^\mu\Big) + J^{lab}_{+1}e^\mu_{+1} + J^{lab}_{-1}e^\mu_{-1} \tag{A.29}$$

Where $J^{lab}_{\pm 1}$ is simply defined from $J\cdot e^\mu_{\pm 1} = -\sum_i J^i e^{*i}_{\pm 1}$.

Since in the non-relativistic limit $P^\mu - \frac{P\cdot q}{q^2}q^\mu = \frac{P^\mu + P'^\mu}{2}$ and $q^2 = -\boldsymbol{q}^2_{lab}$, the nuclear charge and current tensor matrix element is now written as

$$\begin{aligned} \rho_{\lambda'\lambda}(q) &= \rho^{lab}_{\lambda'\lambda}(q) + \mathcal{O}(v^2) \\ J_{\lambda'\lambda}(q) &= \rho^{lab}_{\lambda'\lambda}(q)\frac{P^\mu + P'^\mu}{2m_T} + J^{T,lab}_{\lambda'\lambda}(q) + \mathcal{O}(v^2) \end{aligned} \tag{A.30}$$

Where $J^{T,lab}_{\lambda'\lambda}(q) = J^{lab}_{+1}e^\mu_{+1} + J^{lab}_{-1}e^\mu_{-1}$. Thus the amplitude can be written in the de Forest and Walecka frame

$$T_{fi} = \frac{eg}{\Lambda^2}\boldsymbol{s_T}\cdot\left[\frac{\vec{k}' + \vec{k}}{2m}\rho^{lab}_{\lambda'\lambda}(q) - \Big(\frac{\vec{P} + \vec{P}'}{2m_T}\rho^{lab}_{\lambda'\lambda}(q) + J^{T,lab}_{\lambda'\lambda}(q)\Big)\right] \tag{A.31}$$

This in turn means that the amplitude can be written in terms of the transverse velocity $\boldsymbol{V}_T = \frac{\vec{k}' + \vec{k}}{2m} - \frac{\vec{P}+\vec{P}'}{2m_T}$, where $\boldsymbol{V}_T \cdot q = 0$.

$$T_{fi} = \frac{eg}{\Lambda^2}\boldsymbol{s_T}\cdot\Big[\boldsymbol{V}_T\rho^{lab}_{\lambda'\lambda}(q) - J^{T,lab}_{\lambda'\lambda}(q)\Big] \tag{A.32}$$

## A.4 Cross section

In order to compute the cross section, we first must first calculate $\overline{|T_{fi}|^2}$. Writing in terms of transverse and longitudinal form factors as in [18],[20] and [21] yields

$$\begin{aligned} \overline{\rho^{lab}(q)\rho^{lab*}(q)} &= 4\pi F_L^2(q^2) \\ \overline{\rho^{lab}(q)J^{T,lab,\alpha*}(q)} &= 0 \\ \overline{J^{T,lab,\alpha}(q)J^{T,lab,\alpha'*}(q)} &= 2\pi F_T^2(q^2)\delta_{\alpha\alpha'} \end{aligned} \tag{A.33}$$

With this relation, the amplitude squared is written as

$$\overline{|T_{fi}|^2} = \frac{e^2g^2}{\Lambda^4}\left[\overline{(\boldsymbol{s_T}\cdot\boldsymbol{V}_T)(\boldsymbol{s_T^*}\cdot\boldsymbol{V}_T)}4\pi F_L^2(q^2) + \overline{\boldsymbol{s_T}\cdot\boldsymbol{s_T^*}}2\pi F_T^2(q^2)\right] \tag{A.34}$$

The sum average over spin is written as

$$\overline{\boldsymbol{s_T}\cdot\boldsymbol{s_T^*}} = \overline{(s_i - s\cdot\hat{q}\hat{q}_i)(s_j - s\cdot\hat{q}\hat{q}_j)^*} \tag{A.35}$$

The only contributing factor for the longitudinal form factor will then be

$$\overline{s_is_j^*} = \frac{1}{2}\sum_{s,s'}\xi_{s'}^\dagger\sigma_i\xi_s(\xi_{s'}^\dagger\sigma_j\xi_s)^* = \frac{1}{2}\mathrm{tr}(\sigma_i\sigma_j) = \delta_{ij} \tag{A.36}$$

With the same rule of averaging over initial spins and summing over final spins the contributing factor for the transverse form factor will be

$$\overline{\boldsymbol{s_T}\cdot\boldsymbol{s_T^*}} = \delta_{ij} - \hat{q}_i\hat{q}_j = \sum_{i=1}^{3}\sum_{j=1}^{3}\delta_{ij}\Big(\delta_{ij} - \hat{q}_i\hat{q}_j\Big) = 2 \tag{A.37}$$

Thus the amplitude squared can be written as

$$\overline{|T_{fi}|^2} = \frac{4\pi e^2g^2}{\Lambda^4}\left[\boldsymbol{V}_T^2F_L^2(q^2) + F_T^2(q^2)\right] \tag{A.38}$$

In the center of mass frame we have $\delta(E_{P'}+\varepsilon_{k'}-E_P-\varepsilon_k)d|k'| = \frac{\mu_T}{|k'|}$ and $\mu_T v = k'$, where $\mu_T$ is reduced mass of the target nuclei. Thus eq. (A.4) becomes

$$d\sigma_T = \frac{\mu_T}{4\pi^2k'}\delta(E_{P'} + \varepsilon_{k'} - E_P - \varepsilon_k)|k'|^2d\Omega_{cm}d|k'|\overline{|T_{fi}|^2} \tag{A.39}$$

Integrating then yields the differential cross section

$$\frac{d\sigma_T}{d\Omega_{cm}} = \frac{\mu_T^2}{4\pi^2}\overline{|T_{fi}|^2} \tag{A.40}$$

With the relation $E_R = \frac{\mu_T^2v^2}{m_T}(1-\cos(\theta_{cm}))$, the differential cross section can be written with respect to the recoil energy $E_R$.

$$\frac{d\sigma_T}{dE_R} = \frac{m_T}{2\pi v^2}\overline{|T_{fi}|^2} \tag{A.41}$$

Using the relation $\boldsymbol{V}_T^2 = v^2 - \frac{q^2}{4\mu_T^2}$ we then have the final expression for the differential cross section

$$\frac{d\sigma_T}{dE_R} = \frac{8\pi\alpha}{v^2}\frac{m_T g^2}{\Lambda^4}\left[\left(v^2 - \frac{q^2}{4\mu_T^2}\right)F_L^2(q^2) + F_T^2(q^2)\right] \tag{A.42}$$

where $\alpha = e^2/4\pi$ is the fine structure constant. The longitudinal and transverse form factors are given by eq. (1.22) and eq. (1.28) in [20].

$$\begin{aligned} F_L^2(q^2) &= \frac{1}{4\pi(2J_T+1)}\sum_{M_i}\sum_{M_f}|\rho(q)|^2 \\ F_T^2(q^2) &= \frac{1}{4\pi(2J_T+1)}\sum_{M_i}\sum_{M_f}J_\lambda(q)J^*_{\lambda'}(q) \end{aligned} \tag{A.43}$$

## A.5 Reformulate amplitude in terms of operators

In order to reformulate the amplitude in to the Galilean invariant effective field theory described in section 3.3 we will consider the case of a nuclear spin $J_T = 1/2$. From [18] we have

$$\langle \hat{j}_\mu \rangle = i\bar{u}(P',\lambda')\Big\{\gamma_\mu F_1(q_\mu^2) + \sigma_{\mu\nu}q_\nu F_2(q_\mu^2)\Big\}u(P,\lambda) \tag{A.44}$$

Where $q = P' - P = k - k'$. Thus the matrix element for nuclear current tensor can be written

$$\langle P',\lambda'|\hat{j}^\mu(x)|P,\lambda\rangle = \frac{1}{\sqrt{2E_{P'}2E_P}}\bar{u}_{\lambda'}(P')\Big[F_1(q^2)\gamma' + \frac{i}{2m_T}F_2(q^2)\sigma^{\mu\nu}q_\nu\Big]u_\lambda(P)e^{i(P'-P)x} \tag{A.45}$$

This yields two bilinears

$$\begin{gathered} \bar{u}_{\lambda'}(P')\frac{i}{2m_T}\sigma^{\mu\nu}q_\nu u_\lambda(P) \\ \bar{u}_{\lambda'}(P')\gamma^\mu u_\lambda(P) \end{gathered} \tag{A.46}$$

The first bilinear will in the non-relativistic limit become

$$\begin{aligned} \bar{u}_{\lambda'}(P')\frac{i}{2m_T}\sigma^{\mu\nu}q_\nu u_\lambda(P) &\approx \frac{1}{\sqrt{4m_T}}\Big(\xi^\dagger_{\lambda'}(2m_T + P'\cdot\vec{\sigma}), \xi^\dagger_\lambda(2m_T - P'\cdot\vec{\sigma})\Big) \\ &\cdot\frac{1}{4m_T}[\gamma^\mu,\gamma^\nu]q_\nu\frac{1}{\sqrt{4m_T}}\begin{pmatrix}(2m_T - P\cdot\vec{\sigma})\xi_\lambda \\ (2m_T + P\cdot\vec{\sigma})\xi_\lambda\end{pmatrix} \\ &= \Big(-\frac{q^2}{2m_T}\xi^\dagger_{\lambda'}\xi_\lambda, -i\xi^\dagger_{\lambda'}(q\times\sigma)\xi_\lambda\Big) \end{aligned} \tag{A.47}$$

The second bilinear will in the non-relativistic limit become

$$\begin{aligned} \bar{u}_{\lambda'}(P')\gamma' u_\lambda(P) &\approx \frac{1}{\sqrt{4m_T}}\Big(\xi^\dagger_{\lambda'}(2m_T + P'\cdot\vec{\sigma}), \xi^\dagger_\lambda(2m_T - P'\cdot\vec{\sigma})\Big) \\ &\cdot\begin{pmatrix}0 & \sigma^\mu \\ \bar{\sigma}^\mu & 0\end{pmatrix}\frac{1}{\sqrt{4m_T}}\begin{pmatrix}(2m_T - P\cdot\vec{\sigma})\xi_\lambda \\ (2m_T + P\cdot\vec{\sigma})\xi_\lambda\end{pmatrix} \\ &= \Big(2m_T\xi^\dagger_{\lambda'}\xi_\lambda, -i\xi^\dagger_{\lambda'}(q\times\sigma)\xi_\lambda\Big) \end{aligned} \tag{A.48}$$

Thus the matrix element for nuclear current tensor will be

$$\langle P', \lambda' | \hat{j}^{\mu}(x) | P, \lambda \rangle =$$
$$= (2\pi)^3 \delta^{(3)}(\mathbf{0}) \left( \left[ F_1(q^2) - \frac{q^2}{4m_T^2} F_2(q^2) \right] \xi^{\dagger}_{\lambda'} \xi_{\lambda}, -i \left[ \frac{F_1(q^2) + F_2(q^2)}{2m_T} \right] \xi^{\dagger}_{\lambda'} (q \times \sigma) \xi_{\lambda} \right) \tag{A.49}$$

Inserting this into eq. (A.32) we have

$$\begin{aligned} T_{fi} &= \frac{eg}{\Lambda^2} \left[ \boldsymbol{s} \cdot \boldsymbol{V}_T F_1(q^2) + i \frac{F_1(q^2) + F_2(q^2)}{2m_T} \boldsymbol{s} \cdot (\xi^{\dagger}_{\lambda'} (q \times \sigma) \xi_{\lambda}) \right] \\ &= \frac{eg}{\Lambda^2} \left[ F_1(q^2)(\vec{s}_{\chi} \cdot \vec{v}_T) + i \frac{[F_1(q^2) + F_2(q^2)]}{2m_T} \vec{s}_{\chi} \cdot (\vec{s}_N \times \vec{q}) \right] \end{aligned} \tag{A.50}$$

This demonstrates that the amplitude can be written in terms of a linear combination of the operators $\mathcal{O}_8$ and $\mathcal{O}_9$.

# B

# Source Code

```
In[]:= << "dmformfactor.m"

Welcome to DMFormFactor version 1.1.

Functions are SetCoeffsNonrel, SetCoeffsRel, SetCoeffsNucl, ZeroCoeffs,
  SetJChi, SetMchi, SetIsotope, SetHALO, SetHelm, TransitionProbability,
  ResponseNucl, DiffCrossSection, ApproxTotalCrossSection, and EventRate.

In[]:= ZeroCoeffs[];(*Reset all coefficients*)

In[]:= (*Define Precision for numerical integration and plotting*)
Prec = 10;
SP = 40;
(*Set DM parameters*)
SetJChi[0]; (* Set Spin of DM particle*)
SetMChi[30 GeV]; (*Set mass of DM particle*)

(*Set target parameters*)
AN = 131; (*Isotope Number*)
NP = 54;(*Atomic Number*)
mNucleon = 0.938 GeV; (*Mass of nuclei*)
NT = 1 / (131 mNucleon); (*Number of targets*)

(*Set density of DM*)
Centimeter = (10^13 Femtometer);
rhoDM = 0.3 GeV / Centimeter^3;

(*Set Velocities*)
ve = 232 KilometerPerSecond;
v0 = 220 KilometerPerSecond;
vesc = 550 KilometerPerSecond;
SetHALO["MBcutoff"];

In[]:= (*Set exposure and detector efficiency*)
Exposure = 5.6 * 1000 * KilogramDay * 1000 * 3.3 * 14 / 61.5;
ϵ = 0.7;

In[]:= (*Set Exclusion limit*)
mv = 246.2 ;(*Higgs vacuum expectation value in Gev*)
σex = 4.1 * 10^-47 * Centimeter^2 * GeV^2; (*Excluded cross section limit*)
Cex = 2 * (mv)^2 / (4 * mNucleon * 131 * mNucleon) *
   Sqrt[16 * Pi * (mNucleon + 131 * mNucleon)^2 * σex] * Sqrt[GeV^2];
```

In[ ]:=
```
(*Define dR/dER for relevant operators and xenon target*)
ZeroCoeffs[];(*Reset all coefficients*)
SetCoeffsNonrel[1, c1, 0]
SetCoeffsNonrel[3, c3, 0]
SetCoeffsNonrel[7, c7, 0]
(*Set operator/coupling coefficient with isoscalar coupling*)
SetIsotope[NP, AN, "default", "default"];
dRdER[c1_, c3_, c7_, ERkeV_] = EventRate[1/(AN * mNucleon),
   rhoDM, √(2 * AN * (mNucleon/GeV) * 10^-6 * ERkeV), ve, v0, vesc];
```

Getting default matrix...

Setting isotope to xenon-131.

Your Lagrangian is

$$L_{prot} = 0. + \frac{8.79154\times10^{-6}\ \mathbb{i}\ S_N\cdot(q\times v^{\perp})\ c3}{GeV^3} + \frac{8.24886\times10^{-6}\ 1\ c1}{GeV^2} + \frac{8.24886\times10^{-6}\ S_N\cdot v^{\perp}\ c7}{GeV^2}$$

$$L_{neut} = 0. + \frac{8.79154\times10^{-6}\ \mathbb{i}\ S_N\cdot(q\times v^{\perp})\ c3}{GeV^3} + \frac{8.24886\times10^{-6}\ 1\ c1}{GeV^2} + \frac{8.24886\times10^{-6}\ S_N\cdot v^{\perp}\ c7}{GeV^2}$$

Your event rate is

In[ ]:=
```
(*Redefine dRdER in natural units except keV)*)
dRdERkeV[c1_, c3_, c7_, ERkeV_] = dRdER[c1, c3, c7, ERkeV] * 10^-6 * GeV;
dRdERkeVInterference[c1_, c3_, ERkeV_] =
  (dRdER[c1, c3, 0, ERkeV] - (dRdER[c1, 0, 0, ERkeV] + dRdER[0, c3, 0, ERkeV])) * GeV * 10^-6;
```

In[ ]:=
```
(*Bin looping structs*)
imax = 20; (*Number of bins*)
EminkeV = 5; (*Energy threshold *)
EmaxkeV = 50; (*Max energy*)
deltaBin = (EmaxkeV - EminkeV) / imax; (*Bin size*)

(*Lists for storing the binned energy and rate in*)
E1 = Table[0, {i, imax}];
E2 = Table[0, {i, imax}];
RateO1 = Table[0, {i, imax}];
RateO3 = Table[0, {i, imax}];
RateO1O3 = Table[0, {i, imax}];
RateO7 = Table[0, {i, imax}];
```

In[ ]:=
```
(*Solve for coefficients from exclusion limit
 where the 10^-3 is the suppression of the O3 operator*)
x0 = Solve[NIntegrate[dRdERkeV[Cex, 0, 0, ERkeV], {ERkeV, EminkeV, EmaxkeV},
     WorkingPrecision → Prec] == NIntegrate[dRdERkeV[0, 1, 0, ERkeV],
      {ERkeV, EminkeV, EmaxkeV}, WorkingPrecision → Prec] * c3^2, c3];
x = Solve[NIntegrate[dRdERkeV[Cex, (c3 /. x0)[[2]], 0, ERkeV], {ERkeV, EminkeV, EmaxkeV},
     WorkingPrecision → Prec] == NIntegrate[dRdERkeV[0, 0, 1, ERkeV],
      {ERkeV, EminkeV, EmaxkeV}, WorkingPrecision → Prec] * c7^2, c7];
```

```
In[]:= (*Integrate and calculate rate for each bin*)
Do[
 E1[[i]] = EminkeV + deltaBin * (i - 1);
 E2[[i]] = EminkeV + deltaBin * (i);
 RateO1[[i]] = NIntegrate[dRdERkeV[1, 0, 0, ERkeV],
    {ERkeV, E1[[i]], E2[[i]]}, WorkingPrecision → Prec] * c1^2;
 RateO3[[i]] = NIntegrate[dRdERkeV[0, 1, 0, ERkeV],
    {ERkeV, E1[[i]], E2[[i]]}, WorkingPrecision → Prec] * c3^2;
 RateO1O3[[i]] = NIntegrate[dRdERkeVInterference[1, 1, ERkeV],
    {ERkeV, E1[[i]], E2[[i]]}, WorkingPrecision → Prec] * c1 * c3;
 RateO7[[i]] = NIntegrate[dRdERkeV[0, 0, 1, ERkeV],
    {ERkeV, E1[[i]], E2[[i]]}, WorkingPrecision → Prec] * c7^2;
 , {i, 1, imax}]
NumEventsBinO1O3[c1_, c3_] = (RateO1 + RateO3 + RateO1O3) * Exposure * ϵ;
NumEventsBinO7[c7_] = RateO7 * Exposure * ϵ;

In[]:= (*Define Monte Carlo loop contstructs*)
jmax = 10000; (*Number of samples of q*)

(*Create q stat test vectors*)
qH0 = Table[0, {n, jmax}];
qH1 = Table[0, {n, jmax}];
```

# Bibliography


[1] Rotation curve of spiral galaxy messier 33. `https://creativecommons.org/licenses/by-sa/4.0/`, Accessed on: 2020-05-12.

[2] Wilkinson microwave anisotropy probe. `https://map.gsfc.nasa.gov/`, Accessed on: 2020-05-16.

[3] XENON Collaboration 7. Dark matter search results from a one ton-year exposure of xenon1t. *Phys. Rev. Lett.*, 121:111302, Sep 2018.

[4] Govinda Adhikari et al. An experiment to search for dark-matter interactions using sodium iodide detectors. *Nature*, 564(7734):83–86, 2018. [Erratum: Nature 566, E2 (2019)].

[5] V.I. Arnold. *Mathematical methods of classical mechanics*, volume 60. Springer, 1989.

[6] Rabin Banerjee and Debashis Chatterjee. Non-relativistic reduction of spinors, new currents and their algebra. *Nuclear Physics B*, 954:114994, 2020.

[7] R. Bernabei et al. Final model independent result of DAMA/LIBRA-phase1. *Eur. Phys. J. C*, 73:2648, 2013.

[8] Gianfranco Bertone and Dan Hooper. History of dark matter. *Rev. Mod. Phys.*, 90:045002, Oct 2018.

[9] Gianfranco Bertone, Dan Hooper, and Joseph Silk. Particle dark matter: evidence, candidates and constraints. *Physics Reports*, 405(5):279 – 390, 2005.

[10] A. Boyarsky, M. Drewes, T. Lasserre, S. Mertens, and O. Ruchayskiy. Sterile neutrino dark matter. *Progress in Particle and Nuclear Physics*, 104:1 – 45, 2019.

[11] Riccardo Catena, Alejandro Ibarra, and Sebastian Wild. DAMA confronts null searches in the effective theory of dark matter-nucleon interactions. *Journal of Cosmology and Astroparticle Physics*, 2016(05):039–039, may 2016.

[12] D. G. Cerdeño and A. M. Green. *Direct detection of WIMPs*, page 347–369. Cambridge University Press, 2010.

[13] Marco Cirelli, Eugenio Del Nobile, and Paolo Panci. Tools for model-independent bounds in direct dark matter searches. *Journal of Cosmology and Astroparticle Physics*, 2013(10):019–019, oct 2013.

[14] LUX-ZEPLIN Collaboration. Projected wimp sensitivity of the lux-zeplin dark matter experiment. *Phys. Rev. D*, 101:052002, Mar 2020.

[15] NA48 Collaboration. A new measurement of direct cp violation in two pion decays of the neutral kaon. *Physics Letters B*, 465(1):335 – 348, 1999.

[16] The XENON collaboration. Physics reach of the XENON1t dark matter experiment. *Journal of Cosmology and Astroparticle Physics*, 2016(04):027–027, apr 2016.

[17] G. Cowan, K. Cranmer, E. Gross, and O. Vitells. Asymptotic formulae for likelihood-based tests of new physics. *The European Physical Journal C*, **71**(1554), 2011.

[18] T. de Forest Jr. and J.D. Walecka. Electron scattering and nuclear structure. *Advances in Physics*, 15(57):1–109, 1966.

[19] Scott Dodelson and Lawrence M. Widrow. Sterile neutrinos as dark matter. *Phys. Rev. Lett.*, 72:17–20, Jan 1994.

[20] T W Donnelly and J D Walecka. Electron scattering and nuclear structure. *Annual Review of Nuclear Science*, 25(1):329–405, 1975.

[21] T. William Donnelly and Ingo Sick. Elastic magnetic electron scattering from nuclei. *Rev. Mod. Phys.*, 56:461–566, Jul 1984.

[22] T.W. Donnelly, J. Dubach, and W.C. Haxton. Semi-leptonic weak and electromagnetic interactions in the goldhaber-teller model. *Nuclear Physics A*, 251(3):353 – 384, 1975.

[23] A. Drukier and L. Stodolsky. Principles and applications of a neutral-current detector for neutrino physics and astronomy. *Phys. Rev. D*, 30:2295–2309, Dec 1984.

[24] Leanne D Duffy and Karl van Bibber. Axions as dark matter particles. *New Journal of Physics*, 11(10):105008, oct 2009.

[25] Timon Emken. Dark matter in the earth and the sun – simulating underground scatterings for the direct detection of low-mass dark matter. *arXiv: High Energy Physics - Phenomenology*, 2019.

[26] A. Liam Fitzpatrick, Wick Haxton, Emanuel Katz, Nicholas Lubbers, and Yiming Xu. The effective field theory of dark matter direct detection. *Journal of Cosmology and Astroparticle Physics*, 2013(02):004–004, feb 2013.

[27] Katherine Freese, Mariangela Lisanti, and Christopher Savage. Colloquium: Annual modulation of dark matter. *Rev. Mod. Phys.*, 85:1561–1581, Nov 2013.

[28] Freese, K. Review of observational evidence for dark matter in the universe and in upcoming searches for dark stars. *EAS Publications Series*, 36:113–126, 2009.

[29] D Frisk. A chalmers university of technology master's thesis template for LaTeX. unpublished (parts used from), 2018.

[30] Mark W. Goodman and Edward Witten. Detectability of certain dark-matter candidates. *Phys. Rev. D*, 31:3059–3063, Jun 1985.

[31] G. Hinshaw, D. Larson, E. Komatsu, D. N. Spergel, C. L. Bennett, J. Dunkley, M. R. Nolta, M. Halpern, R. S. Hill, N. Odegard, L. Page, K. M. Smith, J. L. Weiland, B. Gold, N. Jarosik, A. Kogut, M. Limon, S. S. Meyer, G. S. Tucker, E. Wollack, and E. L. Wright. NINE-YEAR WILKINSON MICROWAVE ANISOTROPY PROBE ( WMAP ) OBSERVATIONS: COSMOLOGICAL PARAMETER RESULTS. *The Astrophysical Journal Supplement Series*, 208(2):19, sep 2013.

[32] Bradley Kavanagh, Farinaldo Queiroz, Werner Rodejohann, and Carlos Yaguna. Prospects for determining the particle/antiparticle nature of wimp dark matter with direct detection experiments. *Journal of High Energy Physics*, 2017, 06 2017.

[33] Bradley J. Kavanagh, Riccardo Catena, and Chris Kouvaris. Signatures of earth-scattering in the direct detection of dark matter. *Journal of Cosmology and Astroparticle Physics*, 2017(01):012–012, jan 2017.

[34] J.D. Lewin and P.F. Smith. Review of mathematics, numerical factors, and corrections for dark matter experiments based on elastic nuclear recoil. *Astroparticle Physics*, 6(1):87 – 112, 1996.

[35] F. Mandl and G. Shaw. *Quantum Field Theory*. Wiley, 2013.

[36] A. L. Fitzpatrick N. Anand and W. C. W. Haxton. Model-independent wimp scattering responses and event rates: A mathematica package for experimental analysis. *Phys. Rev. C*, 89:065501, Jun 2014.

[37] Eugenio Del Nobile, Graciela B. Gelmini, Paolo Gondolo, and Ji-Haeng Huh. Direct detection of light anapole and magnetic dipole DM. *Journal of Cosmology and Astroparticle Physics*, 2014(06):002–002, jun 2014.

[38] W. Pauli. Zur Quantenmechanik des magnetischen Elektrons. *Zeitschrift fur Physik*, 43(9-10):601–623, September 1927.

[39] Michael E. Peskin and Dan V. Schroeder. *An Introduction To Quantum Field Theory (Frontiers in Physics)*. Westview Press, 1995.

[40] Chandra X ray Image of 1E 0657-56. Bullet cluster, 2006. `https://chandra.harvard.edu/photo/2006/1e0657/more.html`, Accessed on: 2020-05-11.

[41] J I Read. The local dark matter density. *Journal of Physics G: Nuclear and Particle Physics*, 41(6):063101, may 2014.

[42] Leslie J Rosenberg and Karl A. [van Bibber]. Searches for invisible axions. *Physics Reports*, 325(1):1 – 39, 2000.

[43] Brian D. Serot. Semileptonic weak and electromagnetic interactions with nuclei: Parity violations in electron scattering and abnormal-parity admixtures in nuclear states. *Nuclear Physics A*, 322(2):408 – 438, 1979.

[44] Xiangdong Shi and George M. Fuller. New dark matter candidate: Nonthermal sterile neutrinos. *Phys. Rev. Lett.*, 82:2832–2835, Apr 1999.

[45] Gary Steigman and Michael S. Turner. Cosmological constraints on the properties of weakly interacting massive particles. *Nuclear Physics B*, 253:375 – 386, 1985.

[46] Ira Wasserman. Possibility of detecting heavy neutral fermions in the galaxy. *Phys. Rev. D*, 33:2071–2078, Apr 1986.

[47] S. S. Wilks. The large-sample distribution of the likelihood ratio for testing composite hypotheses. *Ann. Math. Statist.*, 9(1):60–62, 03 1938.